

Spatial Distribution of Lithium in Spodumene-Bearing Pegmatites: A Petrographic and LIBS Analysis

Monique van Veen

Spatial Distribution of Lithium in Spodumene- Bearing Pegmatites: A Petrographic and LIBS Analysis

by

Monique van Veen

to obtain the degree of Bachelor of Science
at Delft University of Technology,
to be defended publicly on Tuesday July 9, 2024 at 11:30 AM

Project Duration: May 21, 2024 – July 9, 2024

Thesis committee:	Dr. T. Schmiedel	TU Delft, Supervisor
	Dr. F. S. Desta	TU Delft, Supervisor
	Dr. K. H. A. A. Wolf	TU Delft



Abstract

With demand for lithium predicted to continue increasing in the coming years, lithium exploration and the development of recovery techniques to extract it will become increasingly important. Lithium is particularly important for the energy transition due to its use in lithium-ion batteries. A major source of lithium are Lithium-Caesium-Tantalum (LCT) pegmatites. Lithium is contained within spodumene crystals and these are therefore the focus of most extraction techniques. The main objective of this study was to create an overview of the lithium distribution in lithium pegmatites based on textural and mineralogical information, combined with elemental analysis using Laser Induced Breakdown Spectroscopy (LIBS). The purpose was to improve the understanding of spodumene characteristics in lithium pegmatites which could affect lithium exploration and recovery.

Six samples from two different lithium pegmatite fields were analysed. Four samples were from the Bergby pegmatite field in Sweden and two samples were from the Bougouni pegmatite field in Mali. Petrographic descriptions were made to understand the mineralogy and textures of spodumene and LIBS analysis was used to measure lithium concentrations across profiles on a micrometre scale. Notable features in the Bergby (Sweden) samples included recrystallised, fine grained spodumene in uneven rims around the primary spodumene crystals as well as in the finer grained groundmass. The average lithium content measured for spodumene from the block samples was between 1.4 to 2.1 wt % Li, which is lower than the commonly measured range for spodumene of 2.8 to 3.5 wt % Li (Aylmore et al., 2018). LIBS analysis on the thin sections was attempted and showed higher average lithium content in the micrometre-scale fractures in the spodumene than in the surrounding spodumene crystal. The results of this thesis show that the majority of the lithium remains contained within primary spodumene crystals in lithium pegmatites but lower concentrations are also present in certain locations in the surrounding rock. Additionally, it indicates that the Keyence EA-300 may not be suitable for Li detection in spodumene crystals due to the significant differences in lithium concentration between thin section and block sample measurements. In future it would be critical to consider factors such as matrix effects, sample preparation and calibration of the Keyence EA-300 for true quantitative analysis of lithium content in spodumene.

Table of Contents

Abstract.....	i
Nomenclature.....	iii
1 Introduction.....	1
2 Literature Review.....	2
2.1 Lithium Pegmatites	2
2.2 Geological History	3
2.2.1 Bergby, Sweden.....	3
2.2.2 Bougouni, Mali	4
2.3 LIBS for use in Li identification	5
3 Methods.....	6
3.1 Optical Microscopy.....	7
3.2 Applying LIBS to the Samples.....	7
4 Results.....	8
4.1 Petrographic Descriptions	8
4.2 LIBS Analysis	15
4.2.1 Keyence EA-300 Properties.....	15
4.2.2 Block Sample Data.....	16
4.2.3 Thin Section Data.....	19
4.2.4 Correlations between different elements in the Spodumene crystals.....	23
5 Discussion	25
5.1 Li Distribution from Mineralogical and Textural Observations.....	25
5.2 Spatial Distribution of Li from LIBS	26
5.3 Li Determination with LIBS – Feasible?	28
6 Conclusion	30
7 Outlook & Recommendations.....	31
Supplementary Data.....	32
References.....	33
Appendix.....	39
Appendix A: Image of the Block Samples.....	39
Appendix B: Spectra for main minerals.....	40
Appendix C: LIBS Average Compositions	42
Appendix D: Additional examples of LIBS profiles through fractures using thin sections.....	44
Appendix E: All LIBS profiles for the Block Samples.....	46
Appendix F: All LIBS profiles for the Thin Sections	50

Nomenclature

Abbreviation	Definition
BB03, BB09, BB11, BB12	Samples from Bergby, Sweden
Fsp	Feldspar
Kfs	Potassium Feldspar
KMM1, KMM2	Samples from Kodal Minerals, Ngoulana, Mali
LA – ICP – MS	Laser Ablation–Inductively Coupled Plasma–Mass Spectrometry
LCT	Lithium – Caesium - Tantalum
LIBS	Laser-Induced Breakdown Spectroscopy
LOD	Limit of Detection
Li	Lithium
Mca	Mica
Ms	Muscovite
PCC	Pearson Correlation Coefficient
Pl	Plagioclase
Qz	Quartz
Spd	Spodumene

1 | Introduction

Demand for lithium (Li) tripled from 2017 to 2022 (IEA, 2023), driven by the transition to renewable energy, its use in electric vehicles and for Li-ion batteries to provide clean energy storage. It has been forecast that demand for Li will be 5 times more than it was in 2018 by 2050 (British Geological Survey, 2021). This highlights the importance for continued Li exploration and recovery. There are two main sources of Li: Li-enriched brines and Li pegmatites (Swain, 2017). Li is found in the mineral spodumene within Li pegmatites. However, literature shows that there can be variation in the Li concentration throughout the spodumene crystal. This may include Li depletion at the crystal edges (Lai et al., 2023) and leaching of Li through fractures in the crystal (Acke et al., 2023). There can also be secondary recrystallisation of spodumene into different textures including fine grained spodumene crystals (Feng et al., 2019). Symplectic textures and fine spodumene can cause issues in the liberation of spodumene during the Li extraction process and therefore causes more Li to end up in tailings. Li extraction is focussed on primary spodumene crystals but quantifying the Li content outside of these crystals may help determine whether more Li could be extracted from pegmatites in future.

The main objective of this study is to create an overview of the Li distribution in Li pegmatites based on textural and mineralogical information, alongside elemental analysis using Laser Induced Breakdown Spectroscopy (LIBS) analysis. These methods are performed on four samples from the Bergby pegmatite field in Sweden and two samples from the Bougouni pegmatite field in Mali. To investigate spodumene characteristics in Li pegmatites and how they could directly affect the spatial distribution of lithium, the following specific research questions will be considered in this study:

1. What textural and mineralogical features are present in and around spodumene crystals?
2. How is Li spatially distributed within spodumene crystals according to LIBS measurements?
3. Can using the Keyence EA-300 (using LIBS detection) provide a quick and inexpensive method to quantitatively map the distribution of Li in a pegmatite sample?

The report begins with a review of literature including the characteristics of Li pegmatites and the processes by which they form, the geologic histories pegmatite fields and theory behind LIBS analysis for Li detection. In the methods, the procedures used during optical microscopy and with the Keyence EA-300 are described. The results begin with the petrographic descriptions of each of the samples. This is followed by the results from the LIBS analysis where the results have been separated based on whether they were measured on the block samples or the thin sections using the Keyence EA-300 elemental analyser. These results will be assessed and related to the research questions in the discussion section. A summary of the findings is given in the conclusions the final chapter contains the recommendations for future research.

2 | Literature Review

2.1 | Lithium Pegmatites

Li pegmatites provide 25 % of the world's Li production (Swain, 2017) and have an average Li content of 1.5 to 4 % Li_2O (Szlugaj et al., 2022). They are very coarse grained igneous rocks and tend to form from melts with a granitic composition (Okrusch & Frimmel, 2020). There are two theories for the formation of pegmatite-forming melt: either by the extreme fractionation of a parental granite intrusion or by partial remelting (anatexis) of a host rock (Koopmans et al., 2023). Chen et al. (2022) concluded that extreme fractional crystallisation of a fertile parental granite was the cause of the enrichment of Li in the melt and subsequent mineralisation of spodumene in the pegmatite. Fertile granites are characterised by being peraluminous, silica-rich and highly fractionated (Breaks et al., 2003). Highly fractionated means that the composition of the residual melt has been altered compared to the original melt by fractional crystallisation. However, this model does not apply in situations where there is no evidence of a parental granite. Knoll et al. (2023) presented a case explained by the anatectic model where a Li-rich pegmatite was likely formed from the partial melting of a Li-rich metasediment and then underwent further fractionation and Li enrichment before crystallisation.

Pegmatite dykes are typically in the order of metres (London, 2014) and are heterogeneous on both a regional scale and internal scale. Zoning can be present on a regional scale, where the more Li-rich pegmatites occur further away (within 10 km) of a parental granite due to increased fractionation with distance (Figure 1) (Breaks et al., 2003). Zoning can also occur internally, ranging from a Li-poor border and wall zone, a Li-rich intermediate zone and often a quartz-rich core (London, 2014).

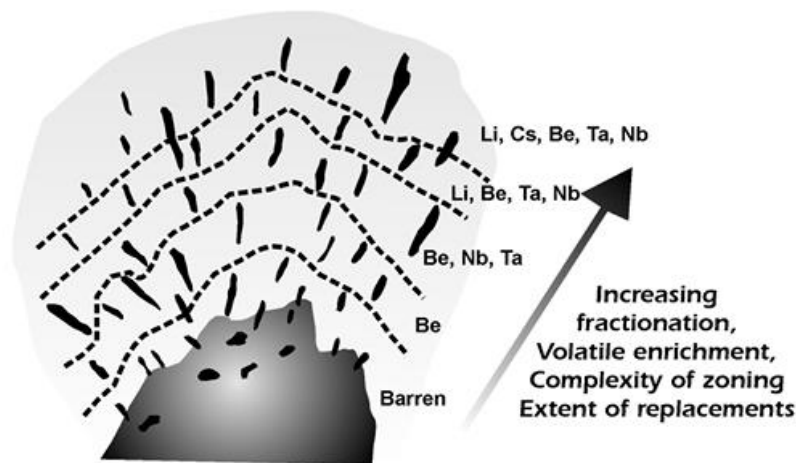


Figure 1. Regional zoning around a parental granite leading to the formation of Li-rich pegmatites (Breaks et al., 2003).

The large crystal size is caused by the enrichment of fluxes (such as F, B and P) and volatiles (water) in the residual melt (London, 2018). They reduce the viscosity of the melt, lower the crystallisation temperature, decrease rates of nucleation and increase rates of diffusion, leading to the growth of large crystals (Phelps et al., 2020; Simmons & Webber, 2008; Thomas et al., 2006). Incompatible elements such as Li also become enriched in these residual melts. The Li is found primarily in spodumene crystals within the pegmatite, but also at lower concentrations in lepidolite, petalite, amblygonite and others (Kundu et al., 2023). Spodumene has the highest theoretical Li content and is often the focus of Li mining (Chen et al., 2022; Kundu et al., 2023)

The NYF-LCT classification (Černý et al., 2005) is one of the most widely used classifications for rare-element enriched pegmatites (Müller et al., 2018). The interest for Li exploration lies with peraluminous LCT (lithium-caesium-tantalum) family of pegmatites, which typically form in orogenic settings from S-type granitic magmas (Černý et al., 2005).

2.2 | Geological History

2.2.1 | Bergby, Sweden

Samples BB03, BB09, BB11 and BB12 were from pegmatite boulders found close to the town Bergby in Sweden. The samples were taken during a field trip associated with the GREENPEG conference in Uppsala 2023. The Bergby LCT pegmatite field (c. 50 km) (Högdahl et al., 2023) was first discovered in 2007 and interest has increased in recent years. Over 9000 m of core drilling has been carried out by United Lithium since 2021 (Leijd et al., 2023). The field guide by Leijd et al. (2023) shows the locations of different pegmatites in the area (Figure 2). Sample BB03 originated from pegmatite A, and samples BB09, BB11 and BB12 are from pegmatite D.

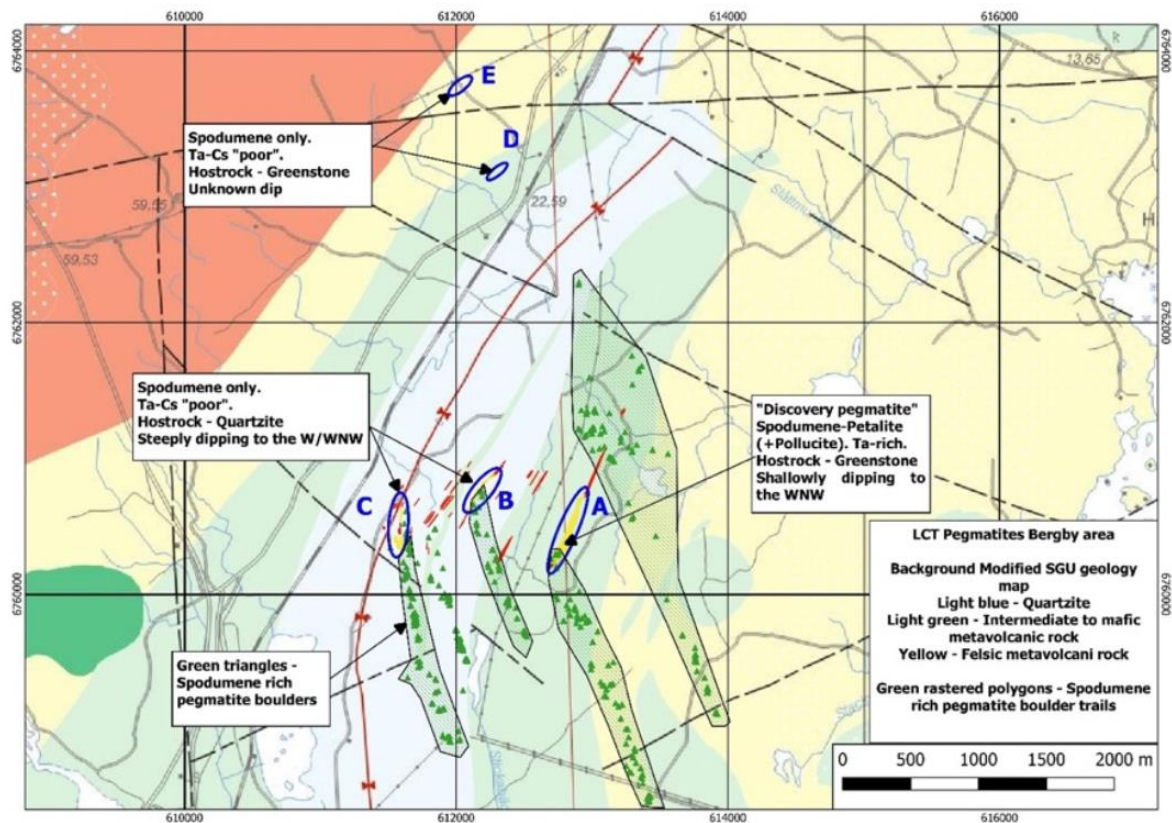


Figure 2. The locations of the different pegmatites in the Bergby pegmatite field overlain on a geologic map of the region (Leijd et al., 2023). Sample BB03 was taken from pegmatite A and samples BB09, BB11 and BB12 were taken from pegmatite D.

This area of Sweden is in the west-central section of the Fennoscandian shield, which is made up of ancient basement rocks that are approximately 2 billion years old (Ga) and formed during the Svecofokarelian orogeny. The Fennoscandian shield is made up of different fragments which originate from different tectonic settings and are separated by steeply dipping ductile shear zones (Högdahl et al., 2009). The Bergby pegmatite field is found within the Ljusdal domain which is bounded to the north by the sedimentary Bothnian basin and by the Bergslagen province to the south (Ogenhall, 2010). The Ljusdal domain consists mainly of granitoids from the Ljusdal batholith (c. 1.86-1.84 Ga) (Högdahl et al., 2009). The Bergby pegmatites are located in the Hamrånge area of the Ljusdal domain. The basic stratigraphy of the Hamrånge area consists of mica schists (1.89 Ga), metavolcanic rocks (1.88 Ga) and quartzites (< 1.855 Ga) (Ogenhall, 2010). The metavolcanic rocks show an oceanic island arc signature whereas the granitoids of the Ljusdal batholith have an active continental margin signature. Ogenhall et al. (2010) suggested that the collision between these two was the first stage of deformation and metamorphism in the area (1.86 Ga) (Högdahl et al., 2009). This was

followed by a period of intra-orogenic extension during which sediments were deposited and later were metamorphosed into quartzite. A second deformation event caused folding and thrusting of the Hamrånge group onto the Ljusdal batholith, alongside a second phase of metamorphism in the amphibolite facies at 1.83 Ga (Högdahl et al., 2009; Leijd et al., 2023; Ogenhall et al., 2010). A final stage of N-S compressional deformation (c. 1.81 Ga) led to the formation of the steep dextral shear zones which cut through the area. The Hamrånge group is cut by the HGZ (Hagsta Gneiss Zone) in the south and the TSZ (Tönnånger Shear Zone) in the north.

The result of these deformation events can be seen in the Hamrånge synform which plunges in an eastern direction (Högdahl et al., 2024) and was formed by first E-W compression and later N-S compression (Ogenhall et al., 2010). The pegmatites in this area were deformed by shearing which took place in 1.81 Ga, meaning that they were emplaced before this event finished. Barren pegmatites are common in the region but LCT pegmatites have thus far only been found within competent host rocks including quartzite and metabasalt (Högdahl et al., 2023). They occur in swarms of LCT pegmatite dykes in the area and have varying compositions. For example, sample BB03 occurred in a pegmatite which was observed to contain both spodumene and petalite, whereas samples BB09, BB11 and BB12 contained only spodumene. Other areas showed large amounts of fine grained Spodumene-Quartz Intergrowths (SQI) (Leijd et al., 2023). The pegmatites are also zoned, with petalite-rich dykes in the centre and decreasing petalite content towards the margins.

2.2.2 | Bougouni, Mali

The KMM1 and KMM2 samples were taken during scout visits in the Bougouni area from the Kodal Minerals Ngoulana target. The Bougouni pegmatite is located in south-western Mali and is one of two key LCT pegmatite swarms, the other being the Goulamina field which is 25 km west of the Bougouni pegmatites (*Bougouni Li Project, Bamako, Southern Mali, West Africa*, 2020). The Ngoulana field has an estimated tonnage of 5.1 Mt and an average grade of 1.2 % Li_2O . Other than the report by Wilde et al. (2021) about the neighbouring Goulamina pegmatites, there is very little literature available about these pegmatites in Mali so their report has been used to give at least some insight into the geologic history of the region.

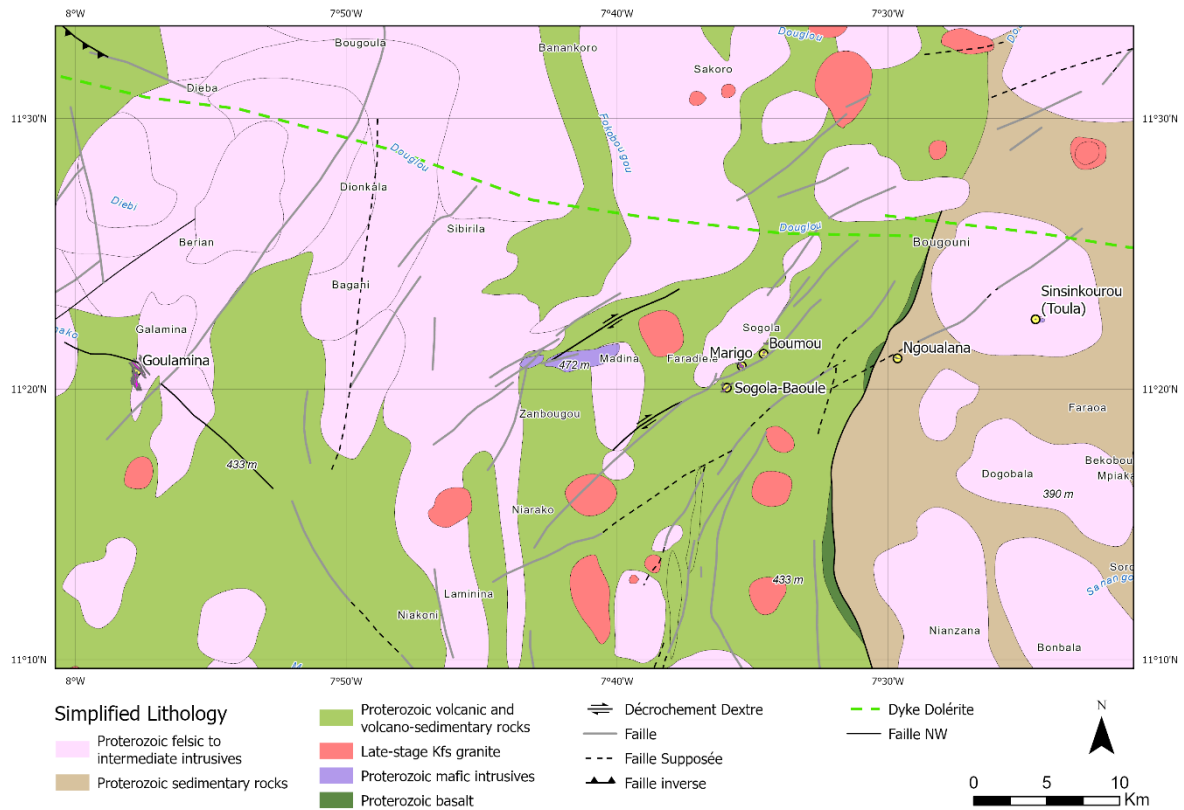


Figure 3. An geologic map of the Bougouni region (West African Exploration Initiative (WAXI), n.d.)

The pegmatites are found in the Baoulé-Mossi domain which is part of the Leo-Man shield (Sanogo et al., 2021). The oldest rocks are of Paleoproterozoic age (dated between 2.19 and 2.13 Ga) and these are the host rocks of the granitoid plutons (including peraluminous granite compositions) and pegmatites in the area. The composition of these host rocks are metavolcanic and metasedimentary and were metamorphosed in the greenschist facies. There were two consecutive intrusion events, the first between 2.25 Ga and 2.1 Ga which give an early arc signature, and the second dated after 2.1 Ga indicating that the first had progressed into a collisional orogen (Wilde et al., 2021). Based on structures measured and analysed by Sanogo et al. (2021) in the Bougouni area, there were three deformation events. The first was NNW-SSE to N-S ductile, low grade metamorphism. This was followed by NNE-SSW to SE-NW ductile-brittle transpressive deformation, corresponding to the emplacement of the majority of the granitoids in the area. A final phase of deformation was E-W oriented and also had a brittle ductile character. Sanogo et al. (2021) suggested that the emplacement of the Bougouni pegmatites were related to this third deformation event.

The Bougouni LCT pegmatites are hosted in the Paleoproterozoic metasediments and amphibolites (Bougouni Li Project, Bamako, Southern Mali, West Africa, 2020). There is extensive lateritic weathering occurring at the surface and it extends to 75 m in the Goulamina pegmatite ore bodies and likely also affects the Bougouni pegmatites. Lateritic weathering can cause the Li to be leached out of the spodumene crystals and it can be recognised in the deposits by a ferricite layer which is extremely iron rich.

2.3 | LIBS for use in Li identification

Laser-Induced Breakdown Spectroscopy (LIBS) is one of the few ways that Li content can be measured directly. LIBS can be used in the lab but also in the field using handheld LIBS. Other advantages of using the LIBS technique are that it requires little sample preparation, provides quick results and produces minimal damage to the sample (Sweetapple & Tassios, 2015). Techniques such as portable XRF cannot be used to measure light elements with an atomic number less than 10, like Li (Sweetapple & Tassios, 2015).

It works by focussing a laser source on an small area ranging between 10 μm and 300 μm in diameter on the surface of the sample. This high energy radiation ablates a small amount of the sample to create plasma which contains ions in their excited states (Müller & Meima, 2022). With cooling of the plasma, light is emitted when electrons fall back down to their ground states, allowing elements to be identified due to the characteristic spectral peaks of the light emitted (Sweetapple & Tassios, 2015). The wavelengths and intensities of the light emitted are measured and recorded using a spectrometer. The intensity of peaks emitted by certain elements is related to the abundance of that element which is present in the plasma (Wise et al., 2022) and can be quantified into weight or molar percentages using calibration curves. Figure 4 gives a schematic overview of the LIBS set up.

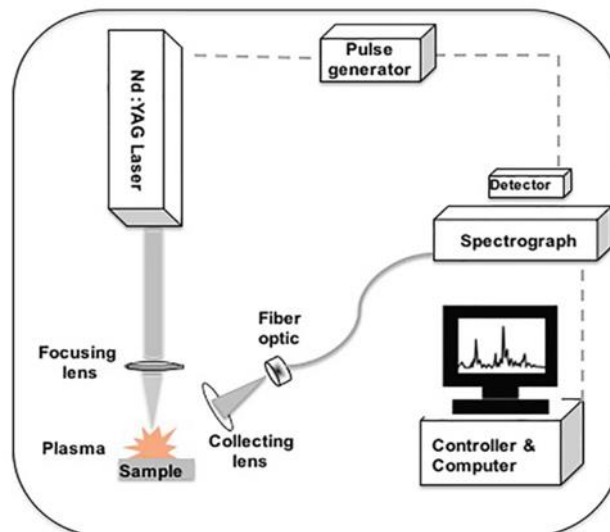


Figure 4. The basic set up of Laser Induced Breakdown Spectroscopy (Senesi & De Pascale, 2022)

Acke et al. (2023) , Fabre et al. (2022) and Müller & Meima (2022) are all examples of LIBS applications in Li pegmatites. Fabre et al (2022) highlighted that LIBS is good for quick identification of Li-bearing minerals in the field when they cannot be identified from visual properties directly. They used rasters of points (spot size of 50 μm) that were averaged for bulk rock analysis. Acke et al (2023) used the LIBS to map Li distribution across a spodumene crystal (100 μm spot size). Müller & Meima (2022) used LIBS to classify minerals in Li pegmatites based on semi-supervised learning by training the model with known reference data (200 μm spot size). Issues with LIBS analysis include matrix effects especially in heterogeneous materials like pegmatites (Müller & Meima, 2022). To quantify LIBS measurements, standards are needed to calibrate the models for each element (Fabre et al., 2022). Calibration curves should theoretically be made for each type of mineral analysed for the specific pegmatite field as each pegmatite field can show differences in their geochemical signature (Dias et al., 2023). Müller & Meima (2022) state that existing LIBS mineral libraries are not transferable between different LIBS systems.

3 | Methods

There were four samples provided from Bergby, Sweden (BB03, BB09, BB11 and BB12) and two samples from Bougouni, Mali (KMM1 and KMM2). Pictures of the block samples can be found in appendix A. The Bergby samples were taken from two different locations within the Bergby pegmatite field, specifically for analysis of the spodumene crystals, not the pegmatite swarm as a whole. The locations of the sampled pegmatites were therefore not taken to be representative of the Bergby pegmatite field. The Bougouni (Mali) samples were taken during scout visits from the Kodal Minerals Ngoulana target. The thin sections were cut from the same sample but with perpendicular orientations with respect to the spodumene crystals.

There were two different methods used in this study. Optical microscopy was used to create petrographic descriptions of each of the samples to allow the mineralogy and textures to be compared. LIBS was used to measure the distribution of Li in the samples over 1D profiles. Detailed explanations of each step are given below.

3.1 | Optical Microscopy

A petrographic description was made for each of the samples. A Leica DM-LP Polarizing Light Microscope was used with 10x/20 mm eyepieces and objective lenses with 5x, 10x, 20x and 50x magnifications. The focus was on the spodumene crystals in each section as these would be measured in the LIBS analysis. Digital scans were also taken of each sample using the Zeiss Axioscan in XPL, PPL and CPL. These are provided in the supplementary material.

A point count was performed on samples BB03, KMM1 and KMM2 to determine modal mineralogy using the Swift Automatic Point Counter Model F. These three thin sections were more representative of the whole rock composition than BB09, BB11 and BB12, where one or two spodumene crystals made up more than 50 % of the sample. 300 points were taken in each point count to obtain representative results. The reliability was determined using the chart by Plas and Tobi (1965). The point counting methods was chosen over multi-label image classification of minerals because it was a time efficient choice for the small number of samples. The use of multi-label image classification would be complex due to the interference colours of each mineral in XPL and overlap between these colours for different minerals in both PPL and XPL. Even in the CPL image, several minerals remain extinct and would therefore not be taken into account in the classification.

3.2 | Applying LIBS to the Samples

For this project, a LIBS detection technique was applied using the KEYENCE EA-300 VHX Series Elemental Analyser. It uses a Nd: YAG 355 nm laser beam with power up to 1 mW and a pulse time of c. 0.1 s to ablate the sample (KEYENCE CORPORATION., 2024). Pre-determined calibration curves that were supplied with the elemental analyser are used to convert the intensities measured into wt % of the elements measured. The results provided by the elemental analyser should be considered semi-quantitative because it has not been calibrated to these samples specifically. The spectra recorded by the elemental analyser were not recorded in the data for the profiles measured, however spectra were taken for the three major components in the samples: quartz, feldspar and spodumene. The size of the points was 10 μm in diameter. There were three options for strength of the laser: weak, medium or strong. All three options were tested on the same profile in the KMM1 block sample. It was chosen to use the “strong” setting for the measurements in this study. It is important to note that any points where an element was not measured by the LIBS was assumed to have a concentration of zero at that location. This made calculations for average composition of spodumene crystals possible.

The elemental composition was measured in profiles across spodumene crystals with a spacing between points of approximately 40 μm on the block samples. A maximum of 25 points could be measured per run so for longer profiles several runs were combined. For these block sample measurements the focus was on the boundaries between spodumene as features like fractures or cleavage planes were not visible in the block samples.

Analysis was carried out on the thin sections using smaller spacings of 12 - 15 μm . These profiles were primarily intended to gather information on any effects of fractures or cleavage planes in the spodumene crystal. The results were categorised based on whether the measurement points were on a fracture or cleavage plane in the spodumene or not. This was determined by examining the pictures taken with the LIBS which recorded the location of each of the measurement points. No distinction was made between fractures or cleavage planes.

Cross plots were used to assess the correlation between different elements in the spodumene crystal. This was quantified using the Pearson Correlation Coefficient (PCC) and was calculated excluding any data for which the Li, Al or Si content was manually set to zero to avoid any bias. The Pearson Correlation coefficients were calculated using equation 1 which was built into the Scipy function “pearsonr” (*Pearsonr — SciPy v1.14.0 Manual*, n.d.).

$$PCC = \frac{\sum_{i=1}^n (x_i - \bar{x})(y_i - \bar{y})}{\sqrt{\sum_{i=1}^n (x_i - \bar{x})^2 \sum_{i=1}^n (y_i - \bar{y})^2}}$$

In order to provide a comparison with both the theoretical composition of spodumene and with other spodumene-pegmatites in literature, a ternary diagram with Li, Al and Si on the vertices of the triangle was plotted in atomic proportions. This required using the average Li, Al and Si content in the spodumene crystals in each sample using the data from the block sample LIBS data. The LIBS gives results in terms of wt % of each element. To convert this into moles, the wt % must be divided by the atomic mass of the respective element. The atomic proportions of Al, Si and Li were calculated by dividing the moles of the individual elements by the total moles of the three elements. The theoretical composition was calculated from the chemical formula of spodumene (LiAlSi₂O₆) (Bradley et al., 2017). Data from other spodumene-bearing pegmatites were taken from the following literature: and Aylmore et al. (2018), Cerny and Ferguson (1972), Charoy et al. (1992) and Dias et al. (2023). Conversions from oxide wt % to elemental wt % was calculated using conversion factors (*Element-to-stoichiometric Oxide Conversion Factors*, 2022).

4 | Results

4.1 | Petrographic Descriptions

In this section, the petrographic descriptions for each of the samples are presented. This includes the mineralogy, quantification from the point count where possible, a description of textures and reference pictures from the thin section scans. The abbreviations for minerals were taken from Warr (2021) and are all listed in the nomenclature section. The following classification was used for crystal sizes: very fine (< 25 μm), fine (25-250 μm), medium (250 – 2500 μm) and coarse (> 2500 μm). Descriptions for the minerals and textures observed were based on the books by MacKenzie et al. (1983) and Mackenzie & Guilford (2014).

Petrographic Description Sheet 1

Sample: BB03

Location: Bergby (Stop 2), Sweden

Mineralogy

Spodumene ($19.6 \pm 4.6\%$) - Shows high relief in PPL compared to quartz and feldspar. Occurs in elongate, lath shaped crystals (subhedral outlines) as well as fine grained, anhedral crystals. One cleavage plane is visible in most cases. Crystal size: 0.2 x 1 cm. There are quartz inclusions in the coarser crystals of spodumene. Has 1st order orange/brown interference colours. The spodumene in the fine grained material has a preferred orientation lengthways with respect to the long side of the thin section. These fine grained spodumene crystals go extinct in clusters.

Quartz ($18.0 \pm 4.5\%$) - Colourless in PPL, 1st order grey interference colour, no cleavage planes. Low relief compared to spodumene. Occurs intergrown with the unknown mineral with lobate boundaries indicating grain boundary migration. Shows undulose extinction. Also occurs in smaller crystals within the finer grained material throughout the section where it has anhedral outlines.

Plagioclase ($20.6 \pm 4.7\%$) - Colourless in PPL but shows brown discolouration indicative of alteration, one set of cleavage planes are visible. Low relief compared to spodumene. Crystals are coarse and have anhedral outlines. Shows albite/lamellar twinning in XPL. 1st order grey interference colours. Appears only on one side of the section, no obvious plagioclase in the fine grained material. Shows sericite alteration.

Mica ($3.3 \pm 1\%$) - Occurs mainly as very fine crystals as an alteration product in and around the feldspar but there are some slightly larger crystals which show one perfect cleavage plane. In XPL, birds-eye extinction is visible in the larger crystals and the interference colours are 3rd order.

Unknown Feldspar ($38.3 \pm 5.7\%$) - Mineral is colourless in PPL and shows little discolouration and has low relief compared to spodumene. One cleavage plane is visible but it is poor. There is no twinning. The interference colours are 1st order grey. Grows around spodumene in a sub-ophitic texture. It is intergrown with quartz with lobate boundaries and contains quartz inclusions (Figure 5). The fractures planes are often filled with quartz.

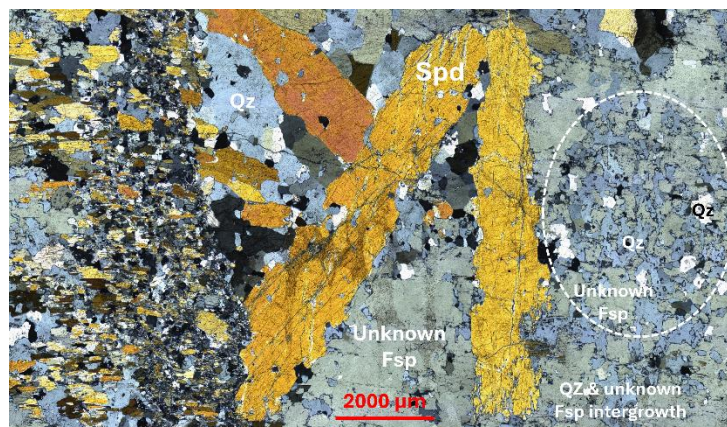


Figure 5. An section of the BB03 thin section viewed under XPL. The fine grained spodumene is visible on the left and the coarser grains of spodumene in centre (Spd). The intergrowth between the quartz (Qz) and unknown feldspar (Fsp) is on the right in the circle indicated.

Textures

Symplectite - Vermicular texture between plagioclase and quartz (quartz blebs within plagioclase on the boundary between plagioclase and the unknown feldspar mineral). (Figure 6A)

Fine grained vein-like material - Occurs at boundaries between the unknown mineral and plagioclase crystals, and in fractures in the unknown mineral. It contains material with orange/brown interference colours as well as grey/white interference colours. (Figure 6B)

Fractures/perthite-like structure - fractures with slight sigmoidal shape which occur in the unknown mineral and are in some cases filled by quartz. (Figure 6C)

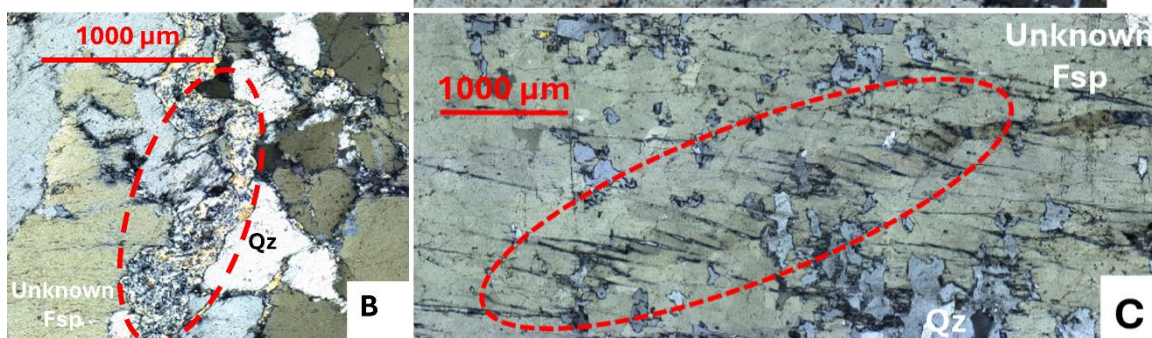


Figure 6. Textures in BB03 viewed in XPL. A: the symplectite texture between plagioclase (Pl) and the unknown feldspar (Fsp). B: the vein-like texture located in the centre of the image. C: The fractures in the unknown mineral, occasionally filled by quartz (Qz).

Petrographic Description Sheet 2

Sample: BB09

Location: Bergby (Stop 4), Sweden

Hand Sample Description:

Outer surface is very weathered and it is covered in very fine grained (clay-like) white material. Pink feldspar (orthoclase) and white feldspar present. Quartz is smoky to white. Spodumene is greenish-beige and typically 2 cm in diameter, length not visible as only part of crystal is present in sample. Micaceous of approx. 0.3 cm. (Figure 7)

Mineralogy

Spodumene - The spodumene crystal makes up about 90% of the thin section. Crystal is has an oval shape, an anhedral outline and its size is 2.3 x 3.5 cm. One set of good cleavage planes visible in PPL. High relief compared to surrounding quartz and feldspar. In XPL, 1st order grey/brown interference colour. Some fractures and cleavage planes are filled with fine grained quartz, feldspar and micaceous. Inclusions of small alkali feldspar crystals

Quartz – occurs as part of the fine grained material and shows undulose extinction.

Plagioclase – Colourless in PPL, shows brown discolouration indicative of alteration, one set of cleavage planes are visible. Low relief compared to spodumene. Crystals have anhedral outlines and are of medium crystal size. Shows albite/lamellar twinning in XPL. 1st order grey interference colours.

Mica – In PPL shows one perfect cleavage plane and low relief compared to spodumene. In XPL, birds-eye extinction is visible in the larger crystals and the interference colours are 3rd order. Fine micaceous in fractures and cleavage planes appear secondary and indicate sericite alteration.

Alkali feldspar - Colourless in PPL, brownish discolouration (alteration) and 1 cleavage plane visible. Shows simple twinning in XPL and 1st order grey

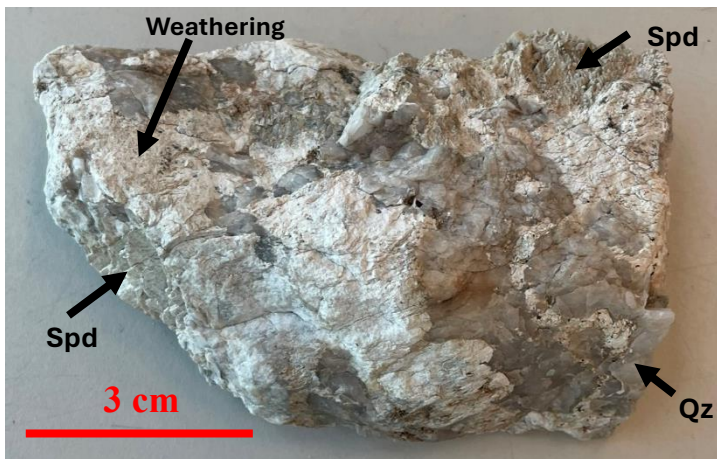


Figure 7. A picture of the hand sample for BB09. Spodumene (Spd) and quartz (Qz) crystals are indicated. The white material on the sample is the weathering product which resides mostly on the feldspars (Fsp).

Textures

Banded, fine grained crystals (crenulations) – Sub-horizontal bands to the spodumene crystal edge of fine grained material. Fine grained material has preferred orientation of approx. 70° to bands (comb texture). Could be crenulation. They are high relief 1st order orange/brown interference colours similar to that of the spodumene crystal. Thickness of bands range from 0.01 to 0.1 cm thick. Thin (approx. 0.01-0.04 cm) rims of this material around spodumene crystal. (Figure 8A)

Alternating very fine grained material and less fine grained quartz and feldspar - Around the edges of the spodumene crystal there is a rim of very fine grained material (Qz – Fsp). This is followed by slightly larger crystals of Qz intergrown with Fsp with sutured boundaries between the two. These two types of layer repeat several times but do not occur on all edges. Sub-horizontal to spodumene crystal boundary. (Figure 8B)

Intergrown feldspars – Shows thin bands of one feldspar inside another. It is not possible to distinguish between lamellar twinning and cross-hatched twinning in the small amount present in the sample. Cross-hatched twinning would indicate microcline. (Figure 8C)

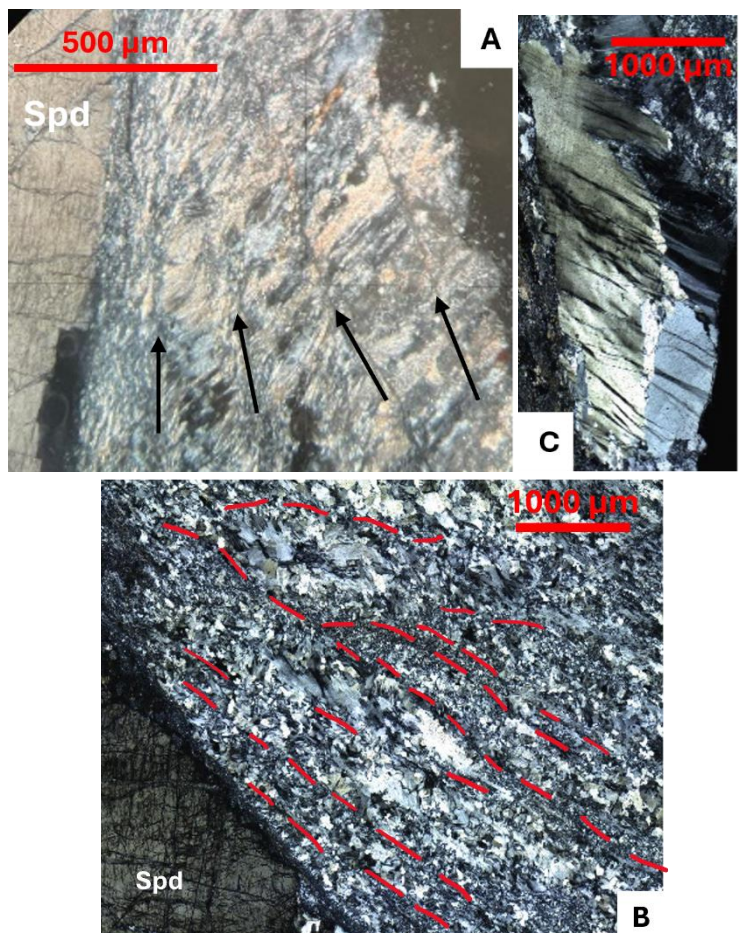


Figure 8. Pictures of the textures in sample BB09 all viewed in XPL. A: the banded fine-grained crystals next to spodumene (Spd). Bands indicated by black arrows. B: The alternating bands (red dashed lines) of very fine and fine grained quartz (Qz) and feldspar (Fsp). C: the feldspar intergrowth.

Petrographic Description Sheet 3

Sample: BB11

Location: Bergby (Stop 4), Sweden

Hand Sample Description:

White feldspar and smoky to white quartz is present. Spodumene is yellowish green and typically 2 cm in diameter, length not visible as only part of crystal is present in sample. Micas present are often greater than 2cm. (Figure 9)

Mineralogy

Spodumene - One main spodumene crystal, subhedral outline. Crystal size: 3.5 x 1.9 cm. High relief compared to quartz and feldspar. One good and one poor cleavage planes visible intersecting at 90 degrees. In XPL, interference colours are 1st order brown/yellow. In the centre of the crystal there is plagioclase present. Smaller crystals with brighter orange interference colours, similar relief, anhedral outlines occur in the fine grained material outside of the main spodumene crystal.

Quartz - No cleavage planes, undulose extinction, anhedral outline. Colourless in PPL, no discolouration. Occur in very fine to medium sized crystals surrounding spodumene crystal.

Plagioclase - Colourless in PPL, low relief compared to spodumene, subhedral outline. Fine to medium sized crystals. Some discolouration visible in PPL - sericitization. In XPL, lamellar/albite twinning visible and 1st order grey interference colours.

Mica - Mostly fine grained surrounding spodumene crystal but one medium sized crystal immediately next to spodumene (pink interference colour). Low relief compared to spodumene. One perfect cleavage plane. Generally 3rd order interference colours (likely muscovite) and birds-eye extinction. Occasionally occurs in lath shapes within other minerals (such as alkali feldspar).

Alkali feldspar - Colourless in PPL, low relief compared to spodumene, subhedral outline. Fine to medium sized crystals. Some discolouration visible in PPL. Two good cleavage planes intersecting at 90 degrees. In XPL, first order grey interference colours and simple twinning.

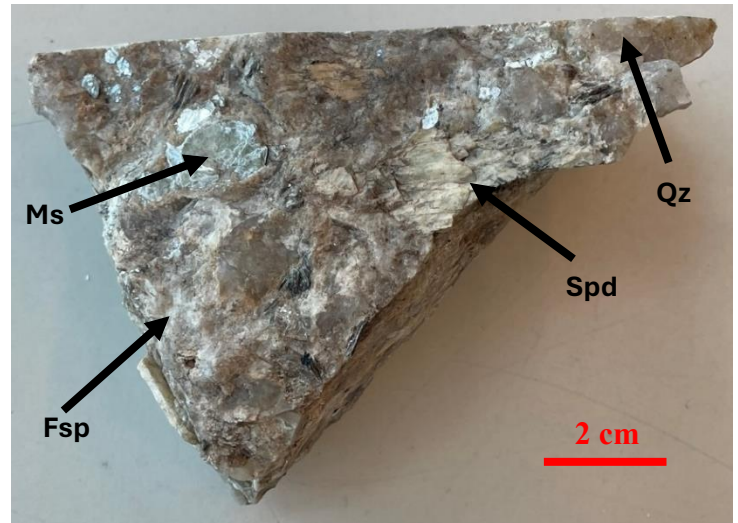


Figure 9. A picture of the hand sample for BB11. Spodumene (Spd), quartz (Qz), feldspar (Fsp) and muscovite (Ms) crystals are indicated.

Textures

Symplectite - Vermicular intergrowth between plagioclase and quartz.

Spodumene needles - Needle shaped spodumene crystals near large spodumene crystal. They do not always occur directly on the edge of the spodumene crystal, it is often separated by fine grained feldspar. In some cases the needles radiate outwards, away from the spodumene crystal. In other cases they are in a comb-like structure in bands with fine grained feldspar, quartz and mica. These bands alternate irregularly but are oriented sub-parallel to edge of the spodumene crystal. Throughout these there are also subhedral larger crystals of feldspar and quartz present. Needle layers are approximately 0.03 cm thick. (Figure 10)

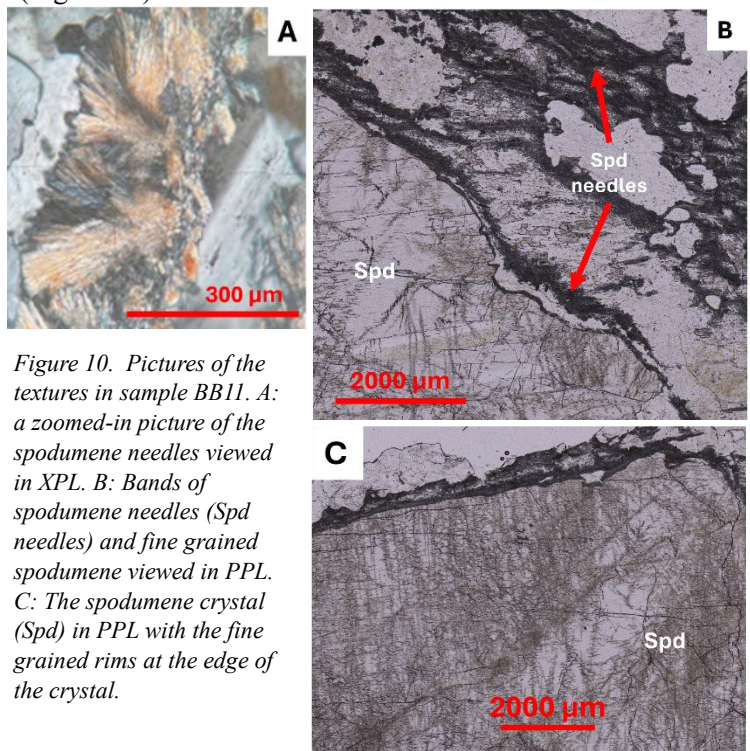


Figure 10. Pictures of the textures in sample BB11. A: a zoomed-in picture of the spodumene needles viewed in XPL. B: Bands of spodumene needles (Spd needles) and fine grained spodumene viewed in PPL. C: The spodumene crystal (Spd) in PPL with the fine grained rims at the edge of the crystal.

Petrographic Description Sheet 4

Sample: BB12

Location: Bergby (Stop 4), Sweden

Hand Sample Description:

Outer surface is very weathered as it is covered in very fine grained (clay-like) white material. White feldspar and smoky to white quartz is present. Spodumene is greenish and typically 2 cm in diameter, length not visible as only part of crystal is present in sample. Micas of approx. 0.3 cm. Black mineral with no distinguishing features may be tourmaline schorl. (Figure 11)

Mineralogy

Spodumene - One main spodumene crystal, crystal size: 2.1 x 1.8 cm, subhedral outline with one perfect cleavage plane. Second spodumene crystal is smaller (Crystal size: 1.1 x 0.3 cm) and show two good cleavage plans intersecting at 90 degrees. High relief compared to quartz and feldspar. Fractures are partially filled with micas – sericitization. In XPL, the interference colours are 1st order grey but large crystal remains very dark. Sharp boundary between spodumene and surrounding minerals. Quartz blebs in the spodumene crystal.

Quartz – No cleavage planes, undulose extinction, anhedral outline. Colourless in PPL, no discolouration. Occur in very fine to medium sized crystals surrounding spodumene crystal.

Plagioclase – Colourless in PPL, low relief compared to spodumene, subhedral outline. Very fine to medium sized crystals, some have subhedral lath shapes. Some discolouration visible in PPL - sericitization. In XPL, lamellar/albite twinning visible and 1st order grey interference colours.

Mica – Mostly fine grained or found within feldspars and spodumene as an alteration product. Low relief compared to spodumene. One perfect cleavage plane. Generally 3rd order interference colours (likely muscovite) and birds-eye extinction.

Alkali feldspar - Colourless in PPL, low relief compared to spodumene, subhedral outline. Very fine to fine sized crystals. Two good cleavage planes intersecting at 90 degrees. In XPL, first order grey interference colours and simple twinning.

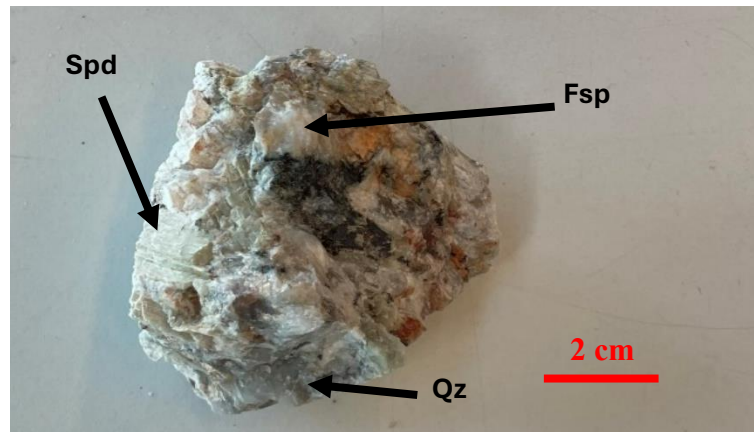


Figure 11. A picture of the hand sample for BB12. Spodumene (Spd), feldspar (Fsp) and quartz (Qz) crystals are indicated.

Textures

Quartz blebs in spodumene – small quartz inclusions in spodumene crystal and occasional vermicular texture on boundary of spodumene and plagioclase. (Figure 12A)

Spodumene needles & fine grained spodumene rims – Needle-like structures in very thin rims around spodumene crystal and larger needle-like structures away from the main spodumene crystal. Needle structures likely spodumene based on interference colours and relief compared to quartz and plagioclase surrounding it. The needles have a radiate habit and have a thickness of 0.05 cm. Rims of with similar features (looks like fine grained spodumene) occur around the spodumene crystal but are thinner, thickness of 0.01 cm. (Figure 12B)

Replacement of crystals by very fine grained quartz - crystals shapes filled with very fine grained quartz and feldspar and minor sericite. Saccharoidal-like texture in some places where quartz crystals are more elongated and surrounded by anhedral groundmass. (Figure 12C)

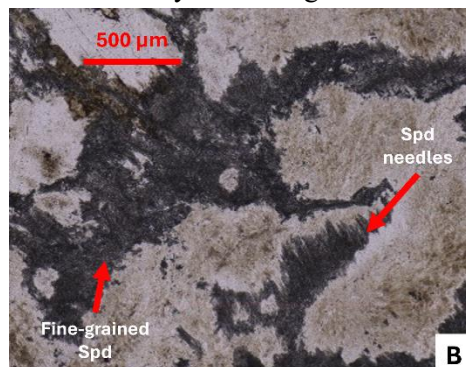
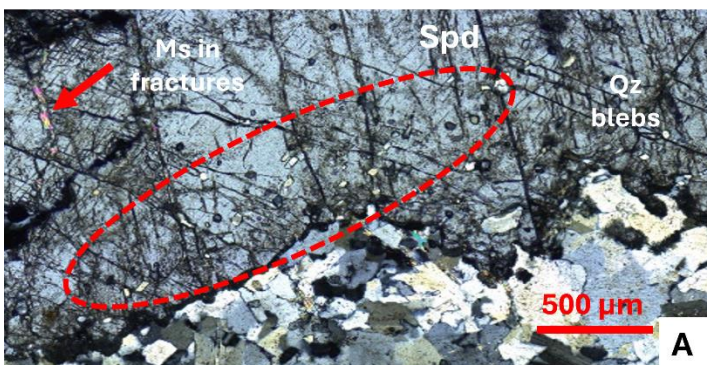


Figure 12. Pictures of the textures in sample BB12. A: Quartz (Qz) blebs inside the spodumene (Spd) crystal and muscovite (Ms) within the fractures in the spodumene crystal. Viewed in XPL. B: Spodumene needle like structures and fine grained spodumene viewed in PPL. C: Grain-like shapes filled with very fine grained Qz – Fsp. Some sericite present identified by high birefringence colours.

Petrographic Description Sheet 5

Sample: KMM1

Location: Bougouni, Mali

Hand Sample Description:

Green spodumene crystals that are > 2 cm long. Muscovite crystals are 0.1 – 0.3 cm. Quartz was colourless to smoky while feldspars were white. Crystal sizes for both feldspar and quartz are around 0.5 cm. There is some brownish discolouration on outside of feldspars. (Figure 13)

Note. Spodumene is parallel to long axis of the thin section.

Mineralogy

Spodumene ($26.6 \pm 5\%$) - Two main, elongated spodumene crystals (Crystal size: 3,9 x 0.3 cm and 1.5 x 0.5 cm) with euhedral to subhedral outlines, High relief compared to quartz and feldspar. Shows one good cleavage plane. In XPL, 1st order yellow to brown/orange interference colours and both crystals show twinning. The boundaries with the other minerals are generally sharp and there are no fine crystals of spodumene.

Quartz ($31.3 \pm 5.4\%$) – 1st order grey to yellow interference colours, low relief compared to spodumene, anhedral outlines and no visible cleavage planes. Lobate boundaries with intergrowth with feldspar. Quartz crystals occur inside spodumene crystals in a poikilitic texture. Shows undulose extinction.

Plagioclase ($31.3 \pm 5.4\%$) – Both coarse and fine crystals. With subhedral or anhedral outlines. Colourless in PPL, low relief compared to spodumene, subhedral outline. In XPL, lamellar/albite twinning visible and 1st order grey interference colours. Twins show some deformation as they are not perfectly straight. Shows undulose extinction. There has been some sericite alteration on the plagioclase crystals.

Mica ($9.0 \pm 3.3\%$) – Laths of mica are common in the section and have subhedral outlines. They have a low relief compared to spodumene and show one perfect cleavage plane. In XPL they have 3rd order interference colours (therefore possibly muscovite) and show birds-eye extinction. (Figure 14C)

Alkali feldspar (1.3 %) - Both fine and coarse crystals. Colourless in PPL, low relief compared to spodumene, subhedral to anhedral outline. Very fine to medium sized crystals. One visible cleavage plane. In XPL, first order grey interference colours and simple twinning.

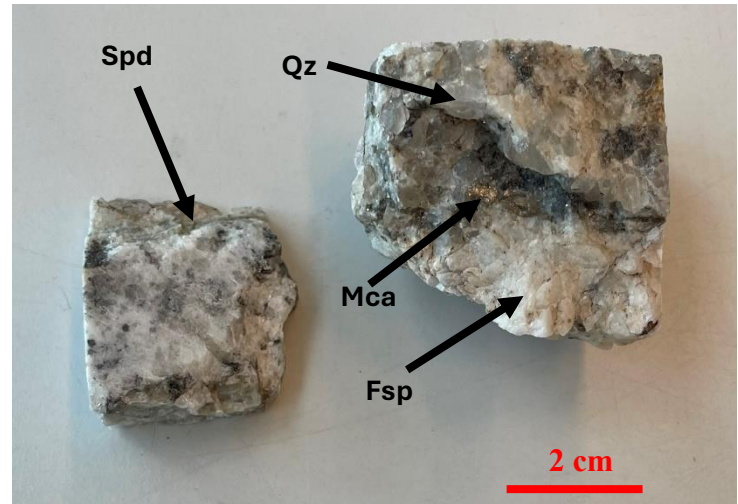


Figure 13. A picture of the hand sample for BB12. Spodumene (Spd) crystal visible on top of smaller sample is indicated as are quartz (Qz), mica (Mca) and feldspar (Fsp).

Textures

Symplectite - Vermicular texture between spodumene and quartz. Does not occur around the entire spodumene crystal.

Quartz blebs and crystals inside spodumene crystal – small quartz inclusions in spodumene crystal as well as some larger crystals of quartz inside spodumene crystal. (Figure 14A)

Spodumene needles – very small number of needle like structures on the very edge of thin section, not visible elsewhere in section. (Figure 14B)

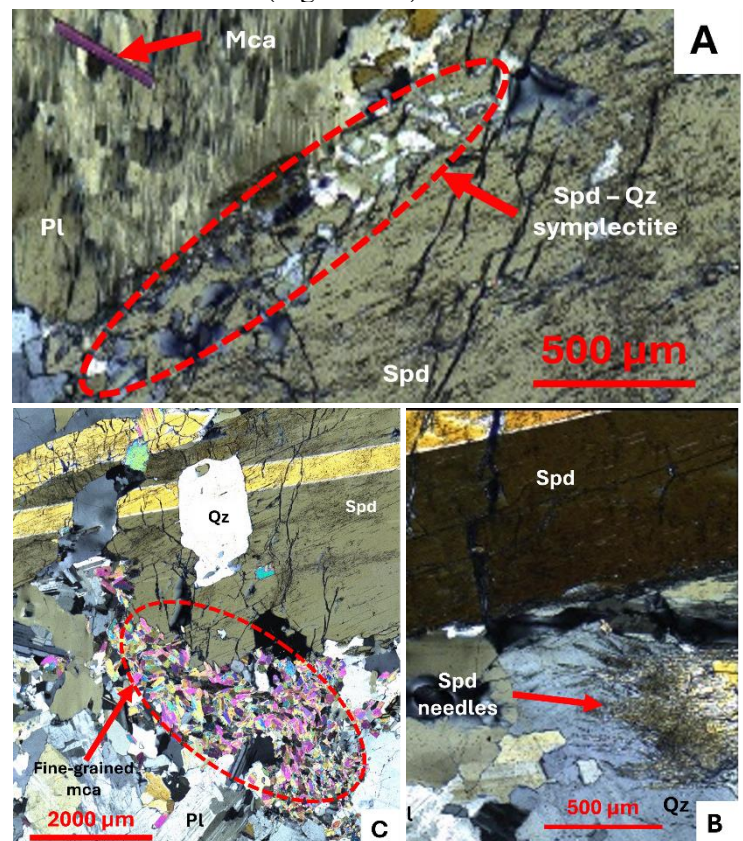


Figure 14. Pictures of the textures and mineralogy in sample KMM1. A: Quartz (Qz) - spodumene (Spd) symplectite texture. Mica (Mca) and plagioclase (Pl) also labelled. Viewed in XPL. B: Spodumene needle like structures next to larger spodumene crystal viewed in XPL. C: Spodumene crystal with quartz crystal inside it and fine grained mica (mca) around the spodumene crystal. Viewed in XPL.

Petrographic Description Sheet 6

Sample: KMM2

Location: Bougouni, Mali

Hand Sample Description: *See hand sample description for sample KMM1.*

Note. Spodumene is orthogonal to long axis of the thin section.

Mineralogy

Spodumene ($22.3 \pm 4.8\%$) - Several oval shaped spodumene crystals with anhedral outlines, high relief compared to quartz and feldspar. Shows two good cleavage planes intersecting at 90 degrees. Crystals diameters are approximately 0.1-0.5 cm. In XPL, 1st order dark grey interference colours and crystals show twinning. Fractures often filled with micas. The boundaries with the other minerals are generally sharp and there are no fine crystals of spodumene.

Quartz ($48.6 \pm 5.7\%$) - 1st order grey to yellow interference colours, low relief compared to spodumene, anhedral outlines and no visible cleavage planes. Quartz crystals occur inside spodumene crystals in a poikilitic texture. Shows undulose extinction.

Plagioclase ($19.3 \pm 4.5\%$) - Both coarse and fine crystals. With subhedral or anhedral outlines. Colourless in PPL, low relief compared to spodumene, subhedral outline. In XPL, lamellar/albite twinning visible and 1st order grey interference colours. Twins show some deformation as they are not perfectly straight. Shows undulose extinction. There has been some sericite alteration on the plagioclase crystals.

Mica ($6.6 \pm 2.5\%$) - Micas are generally in lath-like shapes in the section and have subhedral outlines. They have a low relief compared to spodumene and show one perfect cleavage plane. In XPL they have 3rd order interference colours (therefore possibly muscovite) and show birds-eye extinction.

Alkali feldspar ($2.0 \pm 1.0\%$) - Both fine and coarse crystals. Colourless in PPL, low relief compared to spodumene, subhedral to anhedral outline. In XPL, first order grey interference colours and cross hatched twinning (microcline).

Textures

Symplectite - Vermicular quartz inside spodumene on the boundary of spodumene crystals. Occurs on the majority of the spodumene crystals but not around the entire edge. (Figure 15)

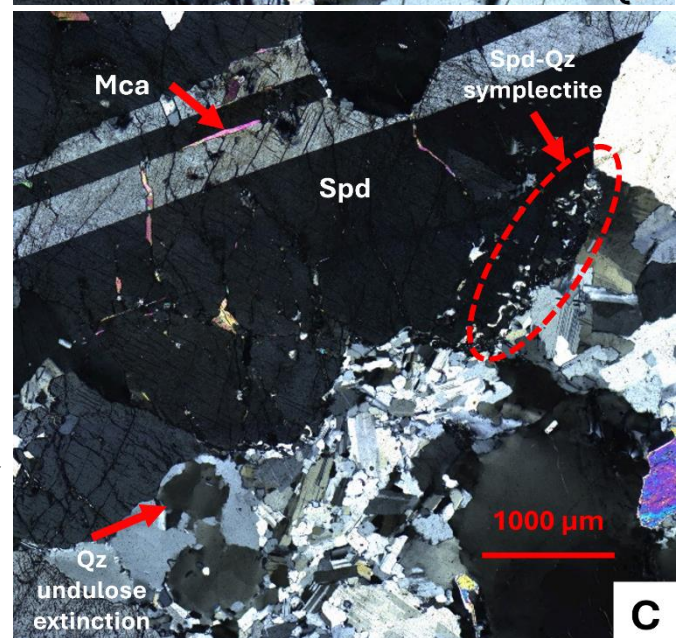
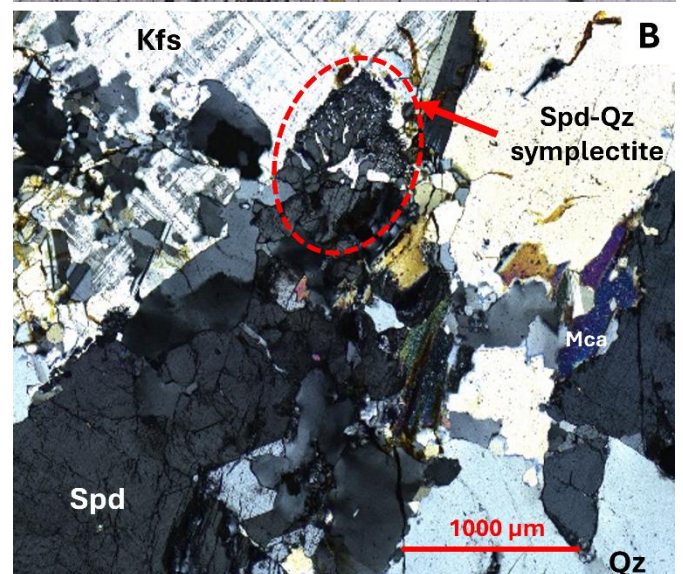
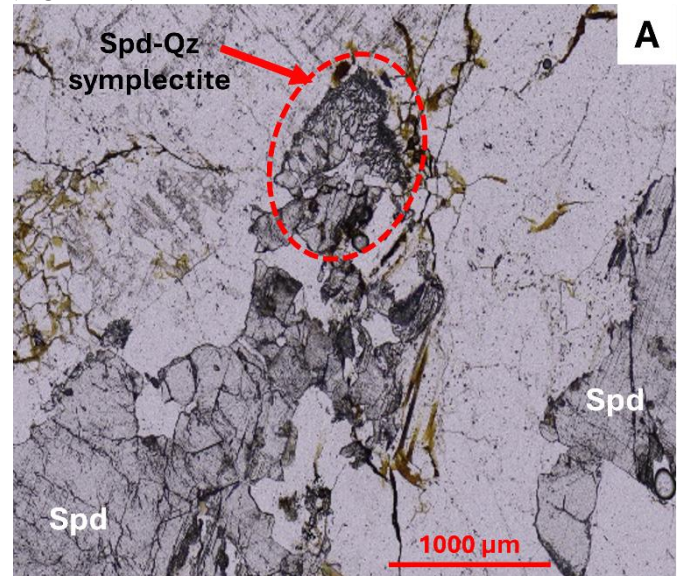


Figure 15. Pictures of the textures and mineralogy in sample KMM2. A: Quartz (Qtz) - spodumene (Spd) symplectite texture viewed in PPL. B: Same quartz - spodumene symplectite texture as in image A but viewed in XPL. Microcline cross-hatched twinning also visible (Kfs). C: Quartz - spodumene symplectite texture viewed in XPL. Mica (Mca) and quartz (Qz) undulose extinction also visible and labelled.

4.2 | LIBS Analysis

In this section the results of the LIBS analysis are presented. This has been separated into data collected from the block samples and data collected from the thin sections as the results show significant differences.

4.2.1 | Keyence EA-300 Properties

In order to determine which strong emission lines were used for the elements, spectra were recorded for quartz, feldspar and spodumene individually. These can be found in appendix B. The peaks used for the key elements measured are in table 1. These values correspond to those in found in literature, see for example Fabre et al. (2022).

Table 1. The spectral lines used for element identification for the main elements found in the LIBS analysis.

Si (nm)	O (nm)	Al (nm)	Na (nm)	Li (nm)
251.61	777.42	308.21	589.00	610.36
212.41	777.52	309.27	818.32	670.79
288.16	-	193.59	819.49	812.64
-	-	199.05	-	-

Additionally, tests were carried out to test the function of the three different power settings on the block samples for the laser: weak, medium and strong (Figure 16). Two different profiles were taken on the block samples and they were not changed between tests. The first profile was carried out with the strong setting first, the second profile was tested using the weak setting first. The strong setting measured all the elements continuously across the sample, whereas weak and medium occasionally did not record Li or aluminium (Al) across the tested profiles. The strong setting showed the least variability in results across the profiles.

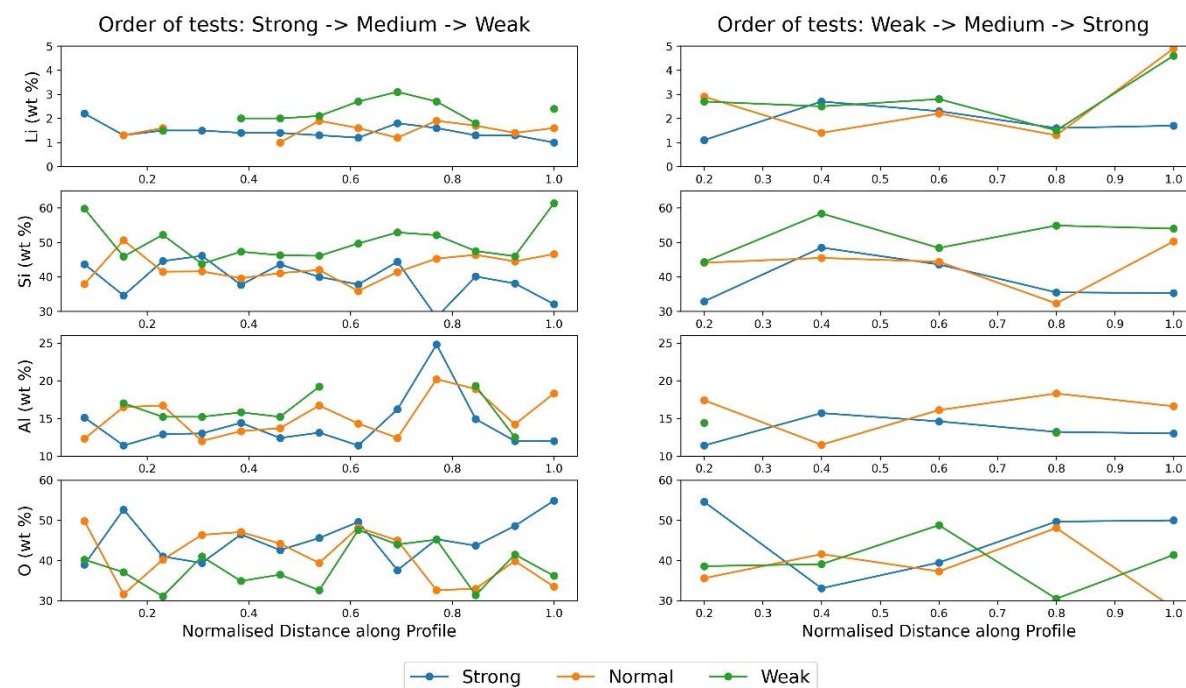


Figure 16. The results of testing the different strength options of the LIBS analyser on two different profiles in KMM1 within a spodumene crystal. The distributions are shown for Li, Si, Al and O, ordered from top to bottom. The left side shows the profile where the strong setting was tested first, followed by the medium and then weak setting. The right side shows a different profile where the tests were carried out in the opposite order.

4.2.2 | Block Sample Data

The data was collected along profiles with a separation between points of approximately 38 μm for the block sample data. In this section, first the Li content across the boundary profiles between quartz or feldspar and spodumene are shown. This data has been focussed on the boundary itself but the full profiles for all the main elements measured can be found in appendix E. This is followed by the boundary profiles passing through rims of intergrown minerals around the spodumene crystal in sample BB11. Finally statistics on the composition of just the spodumene crystals for each sample is presented using the data from all the profiles taken from the block samples.

Block Sample Data - Boundary Profiles

All the boundary profiles of Li content show an increase in Li at the boundary between the spodumene and the neighbouring mineral (Figure 17). Occasionally there is some evidence of Li being present beyond the spodumene crystal, but this does not occur consistently and it cannot be linked to any visual change in the block samples. An exception to this is presented in Figure 18, where a rim could be seen around the spodumene crystal in the block sample.

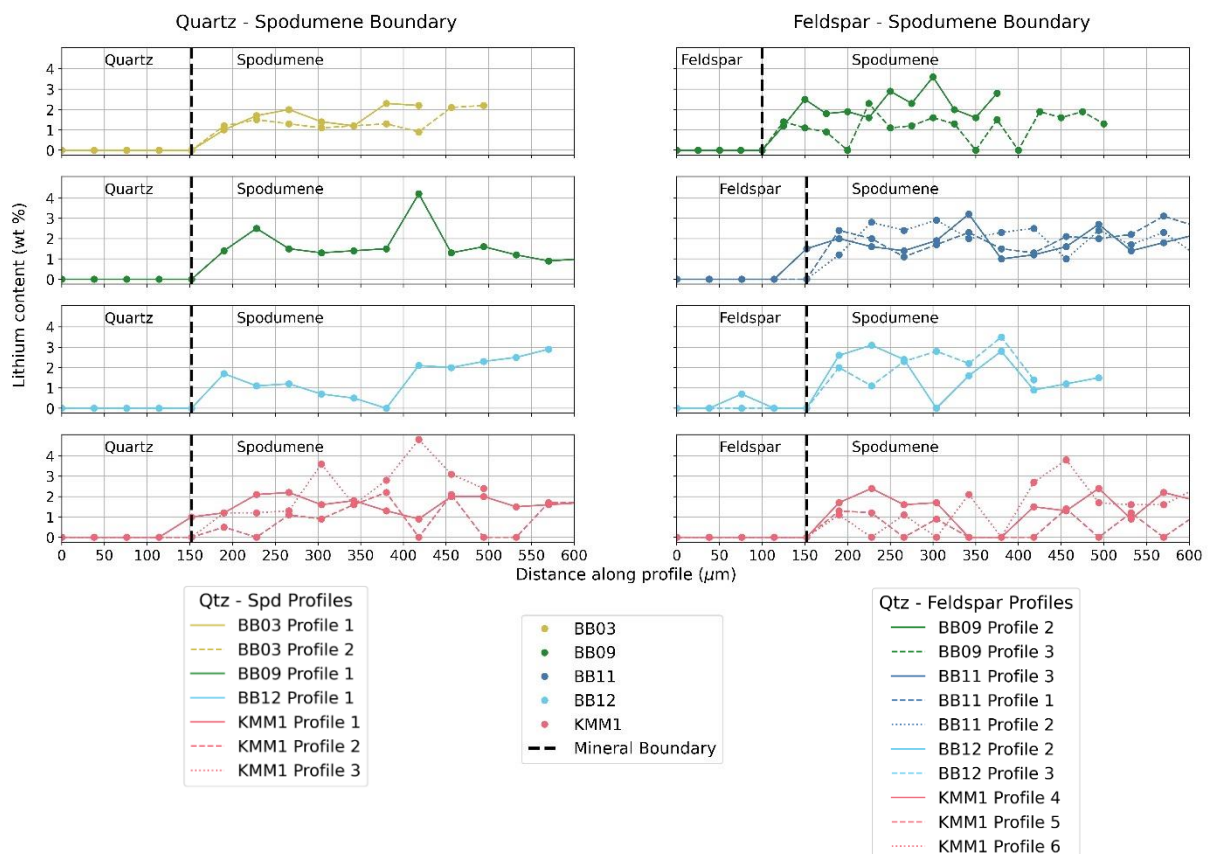


Figure 17. Left: Profiles showing the Li content across the boundaries between feldspar and spodumene for samples BB09, BB11, BB12 and KMM1 from the block samples. Right: Profiles showing the Li content across the boundaries between quartz and spodumene for samples BB03, BB09, BB12 and KMM1 from the block samples. These profiles have been zoomed in on the boundary itself, for the entire profiles see appendix E. Specific profile numbers for each profile in this diagram are provided and correspond to the profile names in the supplementary data.

Block Sample Data - Spodumene Rim Profiles

Figure 18 shows that Li occurs outside of the main spodumene crystal but at an average concentration of 1.7 wt % Li lower in profile 1 and 1.1 wt % lower in profile 2. This occurs in the rim zone around the edge of the spodumene before the composition becomes entirely quartz and feldspar. In this case, the elemental composition of the LIBS of the rim shows it is made up of intergrown Na-rich feldspar and fine grained spodumene. This zone is visible on the block sample itself and the Li content varies

substantially within this rim zone. The thickness of the rim is approximately 1-1.5 mm in this example whereas the spodumene crystal itself is around 3 cm wide. The width and composition of the rim zones varies significantly between samples.

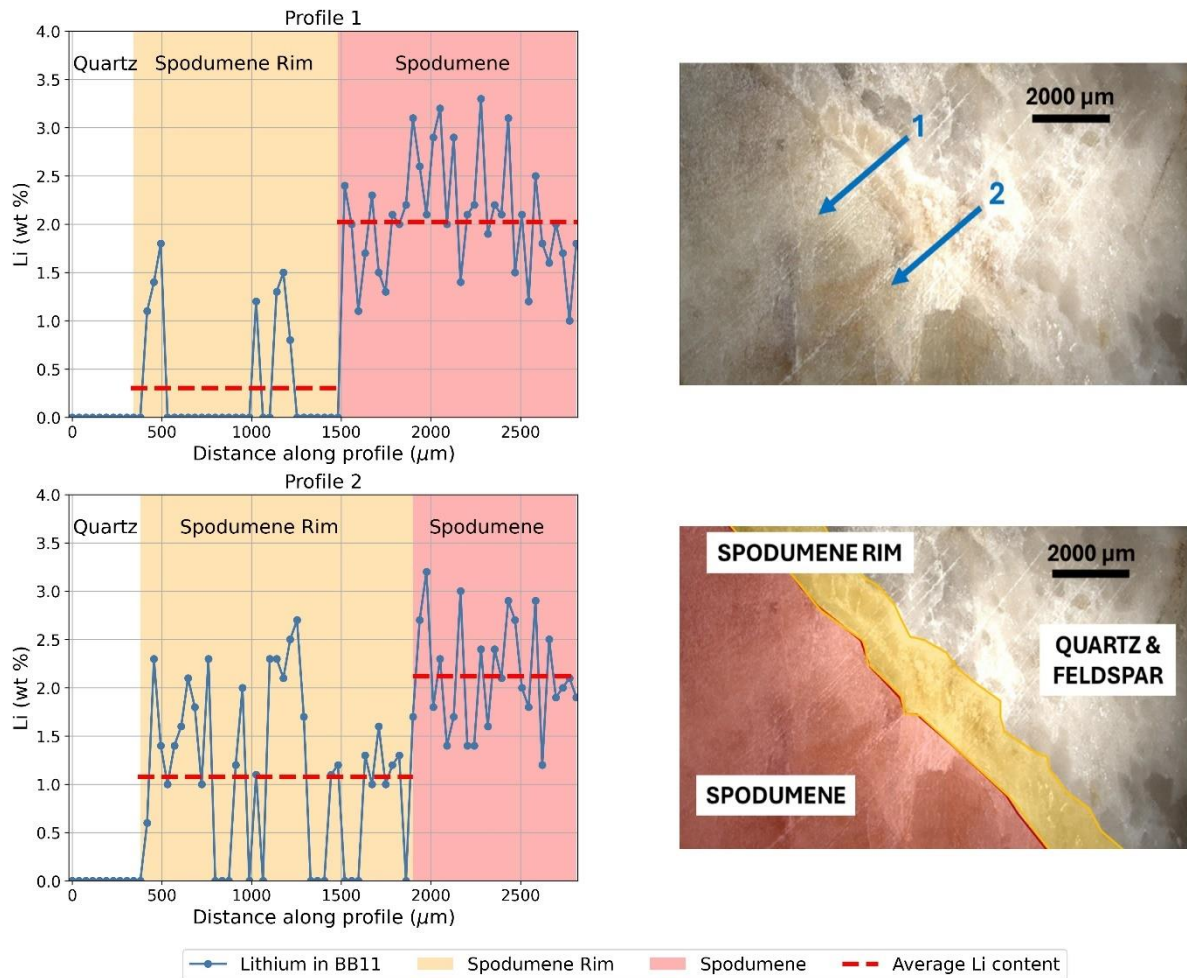


Figure 18. Two profiles through sample BB11 which pass through a rim of Li-bearing mineral before passing into the spodumene crystal. The locations of profiles 1 and 2 are indicated in the image on the top right and the location of the different mineral zones are given in the bottom right image

Block Sample Data - Spodumene Elemental Composition

The elemental composition of the spodumene measured by the LIBS corresponded to its chemical formula $\text{LiAl}(\text{SiO}_3)_2$ (Bradley et al., 2017). Some traces of other elements were measured: K, Na, Au, Ag, Cu, Fe and P. Of these elements, K was the only element that occurred consistently throughout the BB09 sample. The averages and standard deviations for all elements in the spodumene for each sample can be found in tables D1 and D2 (appendix D) and have been summarised in Figure 19. This was calculated using all the available data collected in the spodumene crystals in the profiles.

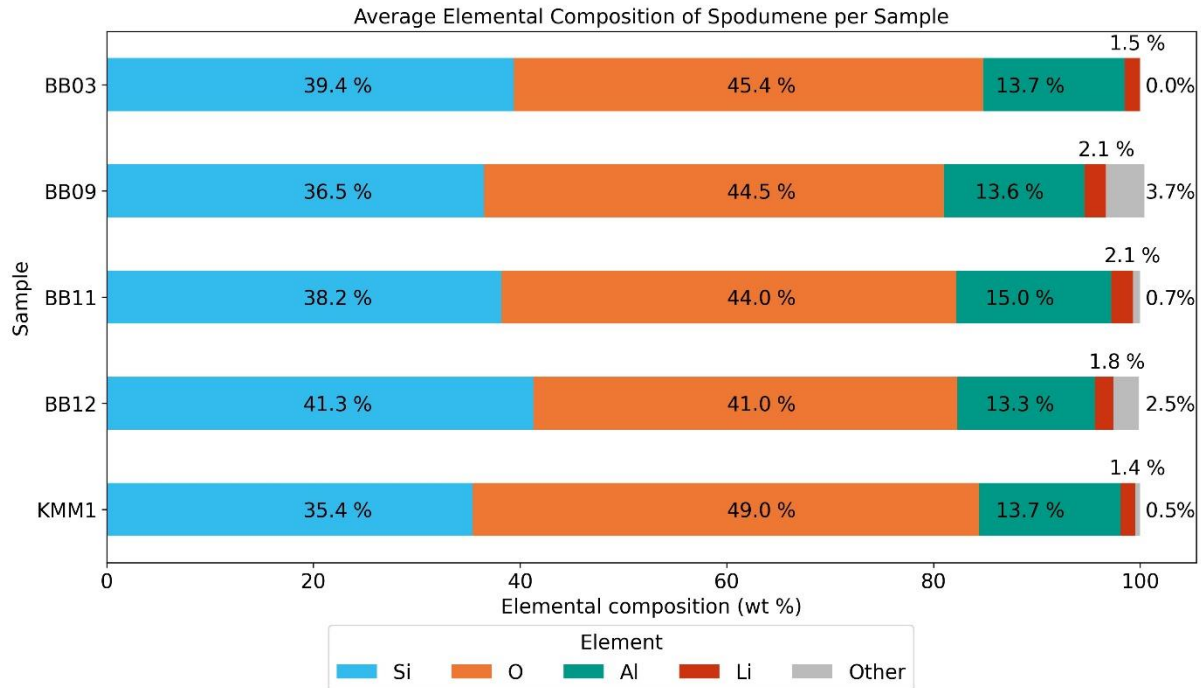


Figure 19. The mean elemental composition of the spodumene in each sample from the block samples. The means were calculated using all data collected that was within the spodumene crystals, including points where no Li was measured which were manually set to zero. The average Li content is given above each bar.

Table 2. Statistics for the Li content in spodumene in each of the samples from the block sample data collected with the LIBS. % zeroes indicate fraction of points within the spodumene crystals where no Li was recorded by the LIBS. % Li was assumed to be zero in these case to make calculations possible. This data was excluded when determining the minimum value for Li.

	Mean	Median	Minimum (excl. manually set zeroes)	Maximum	Standard Deviation	Total number of entries	Number of zeroes	% zeroes
BB03	1.54	1.35	0.9	2.3	0.48	16	0	0.0
BB09	2.09	2.1	0.6	8.3	1.28	404	55	13.6
BB11	2.09	2.1	1.0	4.4	0.83	107	5	4.7
BB12	1.79	2.0	0.5	3.5	0.93	27	2	7.4
KMM1	1.42	1.5	0.5	4.8	1.00	144	31	21.5
KMM2	-	-	-	-	-	-	-	-

Table 2 shows that the Li content is similar between the samples (between 1.4 and 2.1 wt % Li) with KMM1 having the lowest Li content. The percentage of zeroes indicate in what fraction of the points within the spodumene crystals no Li was recorded by the LIBS. At these points the Li content was assumed to be zero to make calculations possible. The highest percentage of zeroes occurs in sample KMM1. No values below 0.5 wt % were measured.

4.2.3 | Thin Section Data

The focus of the thin section profiles was on the internal structures of the spodumene crystal. This was chosen because using the thin sections allowed for fractures and cleavage planes to be visible while doing the LIBS measurements. The data has been categorised on whether a measurement was taken on a fracture in a spodumene crystal or not and the difference in Li content is presented below. Two example profiles are given, additional examples can be found in appendix D. The entire profiles measured on the thin sections are in appendix F. Then the general statistics on the elemental composition of just the spodumene crystals for each sample are presented using the data from the profiles taken from the thin sections.

Thin Section Data - Analysis of Fractures in Spodumene Crystal

The results were categorised based on whether they were taken on a fracture/cleavage plane or not. No distinction was made between fractures or cleavage planes. In all samples analysed, the Li content in the fractures/cleavage planes within the spodumene crystal was higher than in the rest of the spodumene crystal. This difference is greatest in samples KMM1 and KMM2 (Figure 20). This was calculated including the manually set zero values to show an average over the whole spodumene crystal. The differences in statistics caused by the inclusion of these zero values is shown tables in C6 and C7 (appendix C) for both the Li and Al content for the combined samples. Al follows the same pattern as Li.

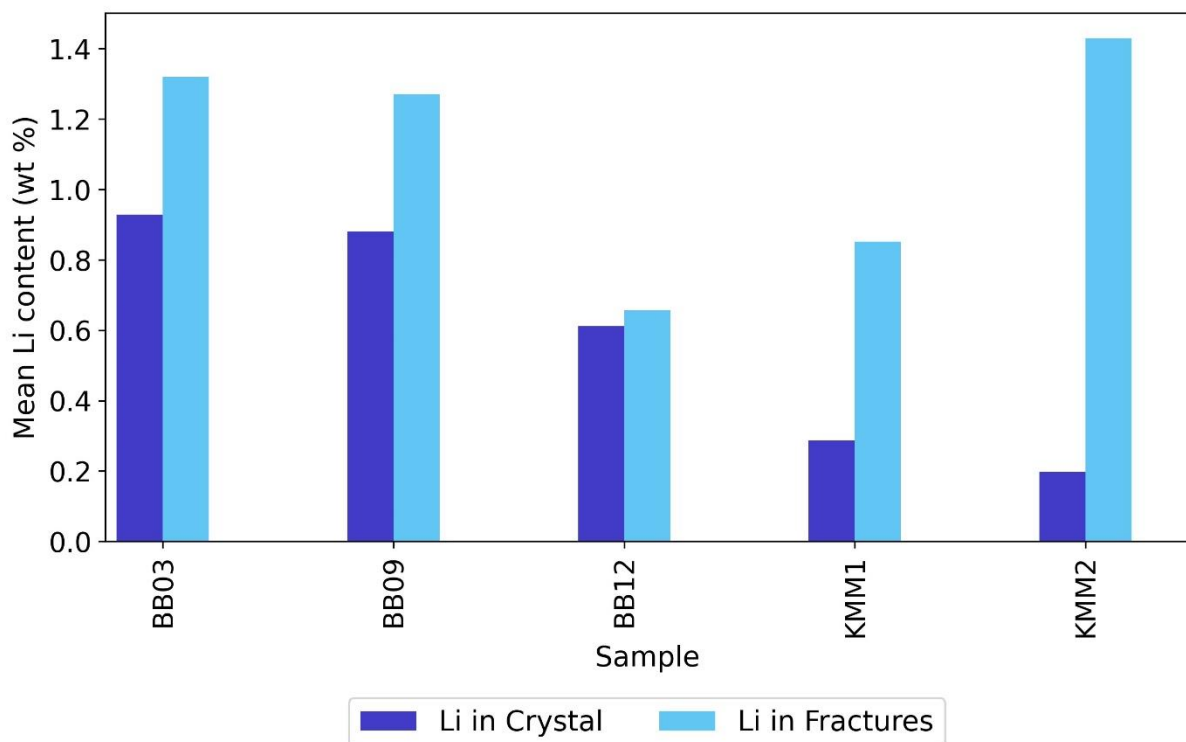
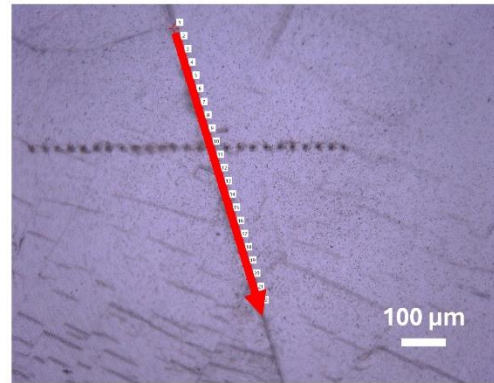
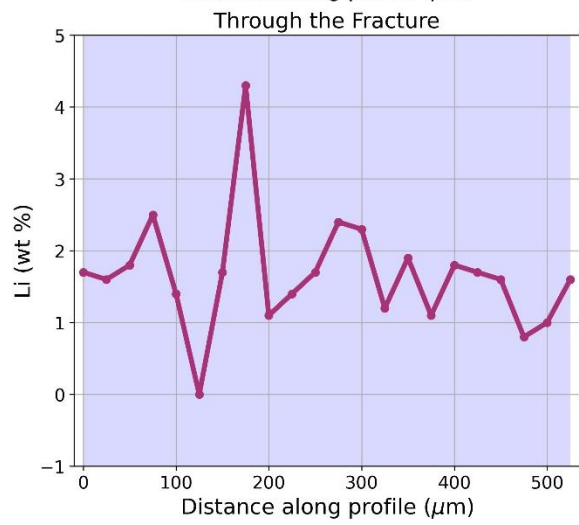
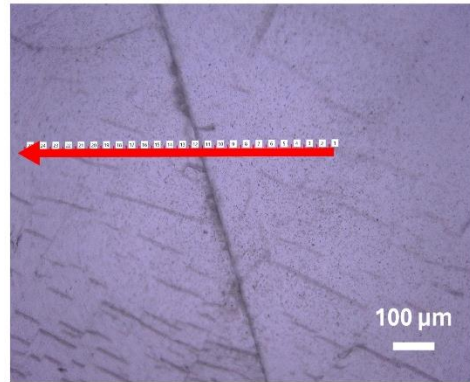
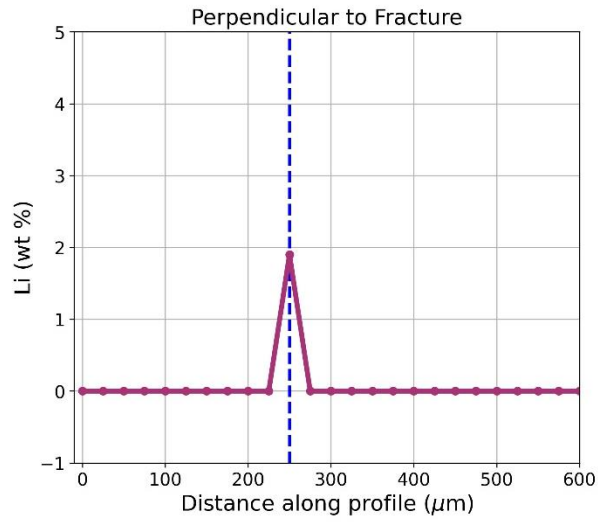


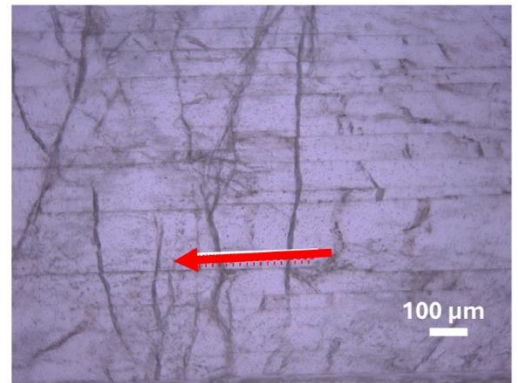
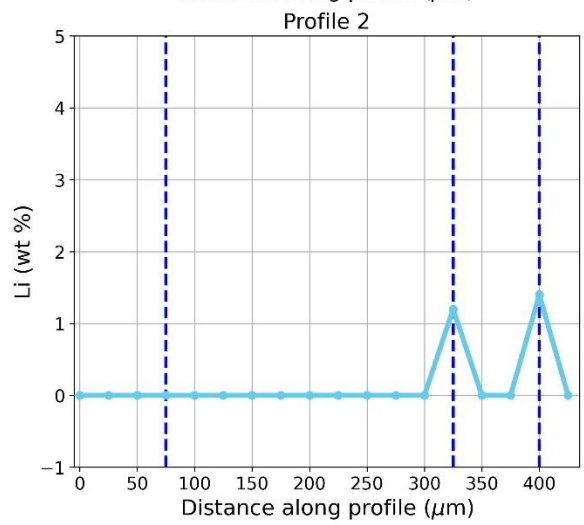
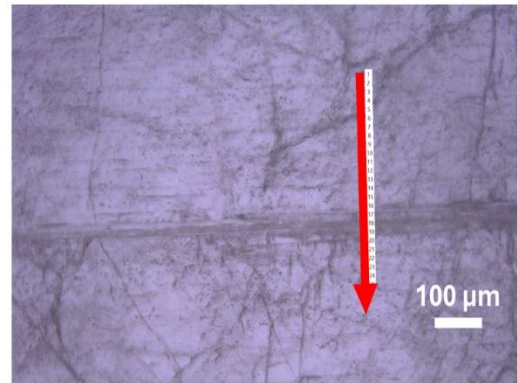
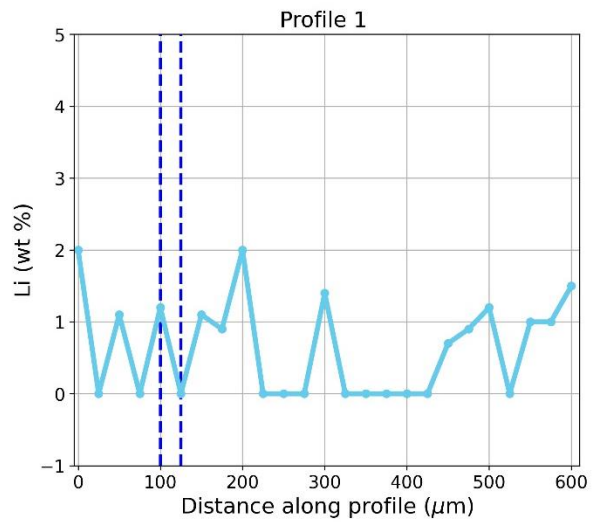
Figure 20. The average Li content for samples BB03, BB09, BB12, KMM1 and KMM2. They have been grouped by being within a fracture/cleavage plane in the spodumene crystal or being in the spodumene crystal itself. Includes points within spodumene crystal where no Li was measured which were manually set to zero to calculate the averages.

Profiles through fractures in the middle of spodumene crystals show Li is in some cases only detected inside the fractures (Figure 21). Other samples show that high Li contents do not always coincide with being measured in fractures (Figures D1 and D2 in appendix D). Figure 22 shows Li is measured more often in profile 1 than profile 2 despite the profiles being taken on the same spodumene crystal in sample BB11. One visible difference between the locations of these profiles is that profile 1 has a “dusty” and more textured appearance compared to profile 2 which looks cleaner.



--- Cleavage Plane or Fracture Within Fracture

Figure 21. Two profiles showing the Li content taken over the same fracture in sample KMM2. Both profiles are taken entirely inside a spodumene crystal. Profile 1 is taken approximately perpendicular to the fracture and profile 2 is taken parallel to and within the fracture itself. The locations of each profile can be seen in the images on the right.



--- Fracture

Figure 22. Two profiles showing the Li content taken over different fractures in sample BB12. The locations of each profile can be seen in the images on the right and the fracture locations on the profiles are marked in blue dashed lines. Both profiles are taken entirely inside a spodumene crystal.

Thin Section Data - Spodumene Elemental Composition

The main elements in the spodumene crystals are Si, O, Al and Li, and traces of other elements include Fe, K, Na and Sn. The K content is again highest in sample BB09. The averages and standard deviations for all elements for each sample can be found in tables C3 and C4 (appendix C) and are summarised in Figure 23. Table 3 shows the statistics for the Li content in the spodumene. The average Li content was between 0.4 and 1.1 wt % Li. The Li content measured by the LIBS was often between 1 and 2 wt % or higher, however the mean was drastically affected by the many measurements within the spodumene crystal where Li was not measured (set to 0 wt % manually as mentioned previously). This can be seen by the percentage of zero values recorded in table 3. For the Bougouni (Mali) samples this exceeded 60 % of the measurements taken in the spodumene crystals.

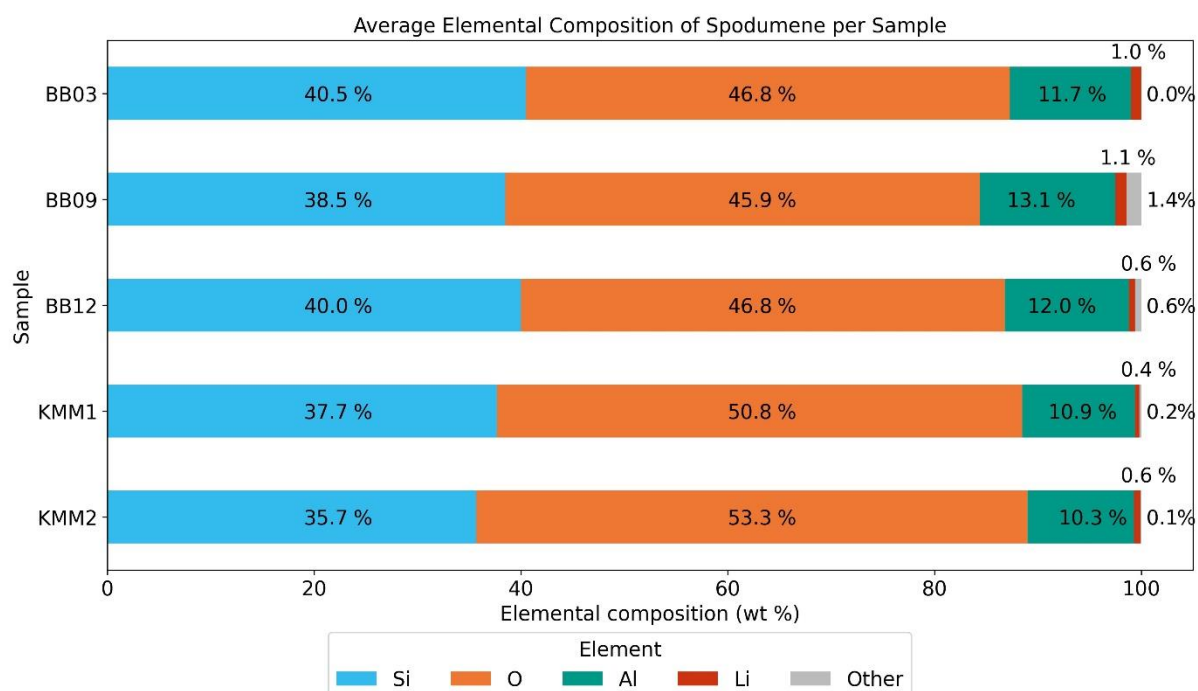


Figure 23. The mean elemental composition of the spodumene in each sample from the thin sections. The means were calculated using all data collected that was within the spodumene crystals including points where no Li was measured which were manually set to zero.

Table 3. Statistics for the Li content in spodumene in each of the samples from the thin section data collected with the LIBS. % zeroes indicate fraction of points within the spodumene crystals where no Li was recorded by the LIBS. % Li was assumed to be zero in these case to make calculations possible. This data was excluded when determining the minimum value for Li.

	Mean	Median	Minimum (excl. manually set zeroes)	Maximum	Standard Deviation	Total number of entries	Number of zeroes	% zeroes
BB03	0.98	1.2	0.8	2.5	0.78	39	13	33.3
BB09	1.06	1.15	0.8	3.1	0.86	106	34	32.1
BB11	-	-	-	-	-	-	-	-
BB12	0.62	0.35	0.7	2.0	0.67	70	35	50.0
KMM1	0.42	0.0	0.8	3.9	0.71	642	456	71.0
KMM2	0.61	0.0	0.8	4.3	0.86	130	82	63.1

4.2.4 | Correlations between different elements in the Spodumene crystals

Cross plots of Al vs Li and Si vs Li measured from the spodumene crystals in the block samples are shown in Figures 24 and 25 respectively. The Pearson Correlation Coefficient (PCC) value is shown in each case. There is a weak to moderate positive correlation (PCC between 0.25 and 0.75) between Li and Al for samples all samples except KMM2. There is no correlation between Li and Si and the PCC from the block samples and thin sections contradict one another. The measurements that had manually set zero values for Li, Al or Si were excluded from this analysis as to not introduce any bias. No Li content is measured below 0.5 wt % Li.

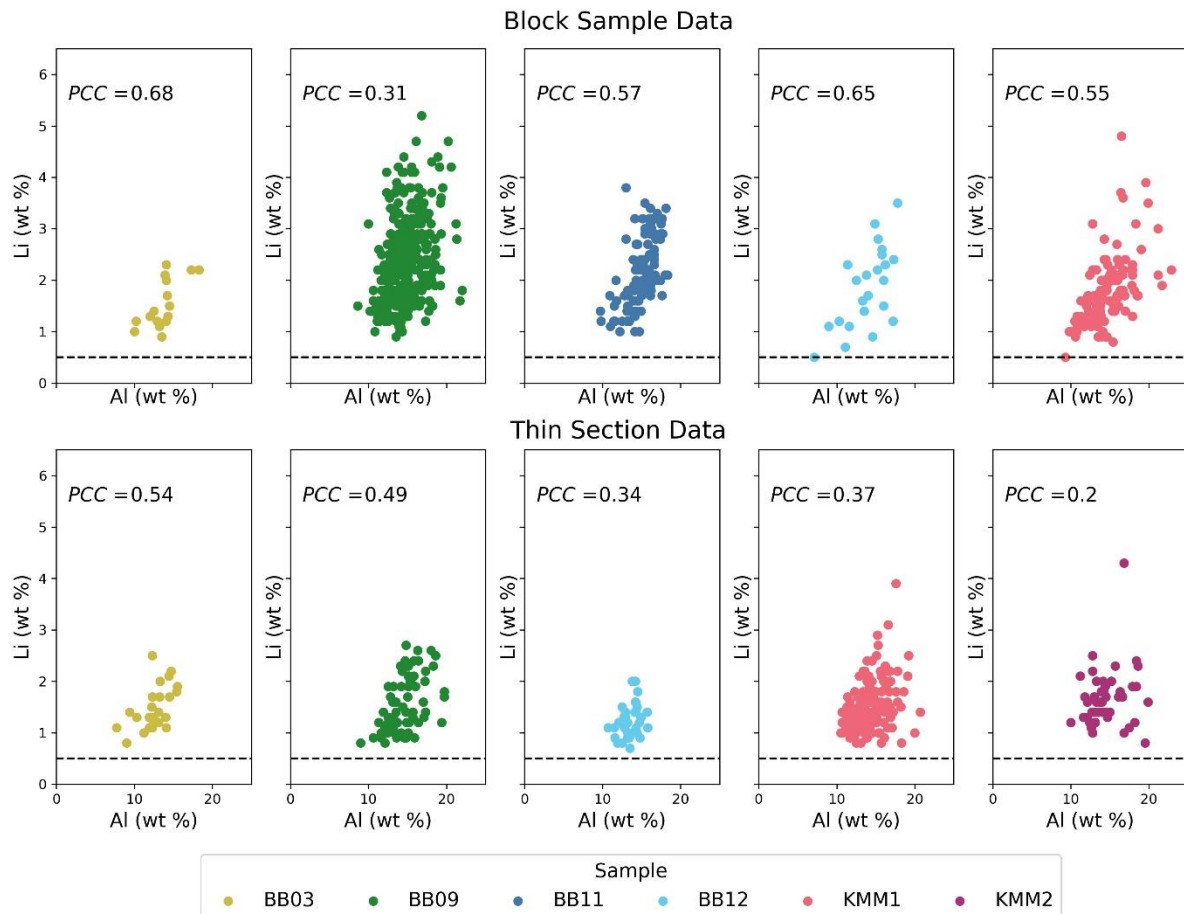


Figure 24 . Cross plots of Al vs Li per sample from the spodumene crystal in the block samples (top) and thin sections (bottom). The PCC value indicates the Pearson correlation coefficient for each case. Black dashed line corresponds to 0.5 wt % Li.

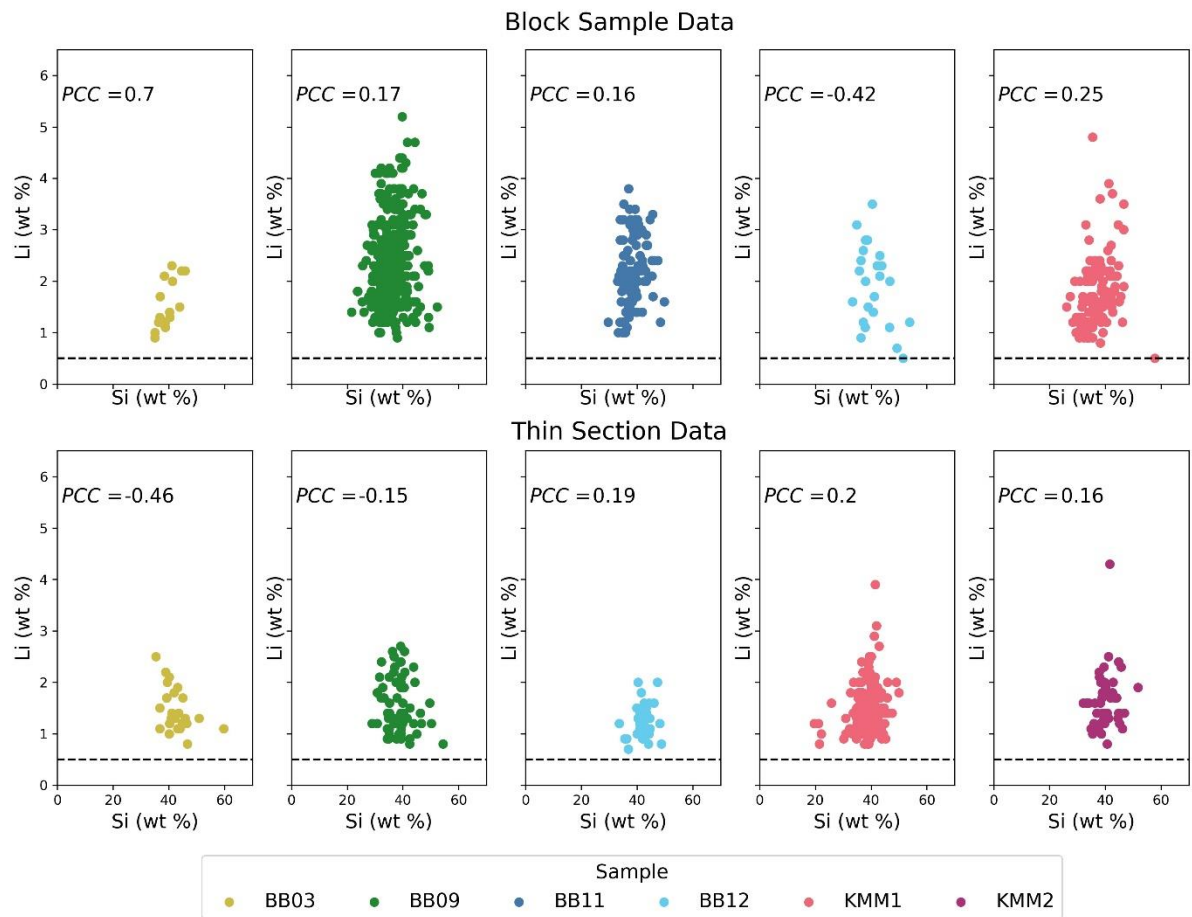


Figure 25 . Cross plots of Si vs Li per sample from the spodumene crystal in the block samples (top) and thin sections (bottom). The PCC value indicates the Pearson correlation coefficient for each case. Black dashed line corresponds to 0.5 wt % Li.

5 | Discussion

5.1 | Li Distribution from Mineralogical and Textural Observations

Three types of spodumene crystals were identified from the petrographic descriptions of the samples. Type 1 were coarse, euhedral spodumene crystals. In KMM1 and KMM2, these generally had distinct, sharp boundaries with other minerals. In the Bergby (Sweden) samples, these boundaries often had a mottled appearance or were surrounded by fine grained rims. The euhedral character of the type 1 spodumene crystals indicates that they crystallised earlier than the sub- to anhedral minerals surrounding them. This is typical for Li pegmatites (Lai et al., 2023). Type 1 spodumene occasionally contain quartz inclusions of varying size ($< 50 \mu\text{m}$ to $1000 \mu\text{m}$). Acke et al. (2023) described these as a primary crystallisation feature due to the observed continuation of cleavage planes into this texture which is also true in this case (Figure 12A). The euhedral character and quartz inclusions within the spodumene indicate the pegmatites' primary magmatic origin.

The type 2 spodumene crystals occur in a vermicular intergrowth with quartz around the rims of the type 1 spodumene crystals. This is most common in sample KMM2 but is also observed to a lesser extent in sample KMM1 and in the Bergby (Sweden) samples. This is a symplectitic texture and indicates a secondary reaction between the primary spodumene and surrounding quartz. Those textures are associated with a hydrothermal origin and are common in LCT pegmatites (Feng et al., 2019; Lai et al., 2023). The pegmatites from both Sweden and Mali show a hydrothermal crystallisation signature.

The third type of spodumene crystals are fine grained, in some cases acicular (needle-like), crystals that occur around the edges of the type 1 spodumene crystals and within finer grained groundmass of other minerals (quartz, feldspar, micas). This occurred primarily in samples BB09, BB11 and BB12. The growth textures of the type 3 spodumene crystals indicate that they are secondary and likely formed from recrystallisation of the type 1 spodumene as a result of hydrothermal alteration. In samples BB09 and BB11, type 3 spodumene occurs in bands resembling crenulations sub-parallel to the edge of the type 1 spodumene. These bands imply at least one deformation event. The final deformation event of the Hamrånge area affected the Bergby pegmatites in 1.81 Ga during a crustal-scale shear event (Högdahl et al., 2024). Acicular spodumene crystals were concluded by Acke et al. (2023) to occur in more deformed zones of the pegmatites. The fine grained rims around the type 1 crystals may have formed as a third generation of spodumene (Feng et al., 2019). This implies that Bergby (Sweden) samples BB09, BB11 and BB12 may have undergone more deformation than BB03. Sample BB03 was taken at a different location to BB09, BB11 and BB12 which may be the cause in this difference in observed textures. The Bougouni (Mali) samples show extremely little type 3 spodumene which suggests they come from a less hydrothermally altered pegmatite. Extraction of Li from type 2 and 3 spodumene creates new challenges as flotation has poor recovery of fine grained spodumene and symplectites (Lai et al., 2023; Xie et al., 2020). The Bergby (Sweden) samples show a stronger hydrothermal crystallisation signature than the Bougouni (Mali) samples.

In the petrographic analysis of sample BB03, 38 % of the sample was made up of a mineral with optical features most resembling a feldspar. It was intergrown with quartz, has anhedral crystal shapes with sutured boundaries and showed simultaneous extinction over large areas. However, the LIBS analysis showed Li was present as well as Al, Si and O (table C5, appendix C) which does not imply that it is a feldspar. Its texture is very similar to a type of spodumene-quartz intergrowth (SQI) described by Thomas et al. (1994). They suggested that the texture formed due to an event post magmatic crystallisation which lead to super saturation in Li, causing the crystallisation of quartz and spodumene at a eutectoid. However the mineral is not spodumene, based on optical properties. Bischoff & Bischoff (1988) suggested that spodumene could later be replaced by eucryptite (LiAlSiO_4) (Bradley et al., 2017) as it is a low temperature alteration product of spodumene (Thomas

et al., 1994). Černý & London (1983) indicate that petalite can also breakdown into eucryptite and quartz intergrowths. Petalite has been recorded in the pegmatite that sample BB03 was taken from (Leijd et al., 2023). Other methods such as short wave UV light could be used to test for eucryptite as it has a pale pink to cream fluorescence (Charoy et al., 2001). Quantitative data for the composition of this mineral would also be useful in identification, for example by using LA-ICP-MS (Rohiman et al., 2023). Another Li-bearing mineral is present in sample BB03 but its composition cannot be derived from the LIBS data but it forms textures similar eucryptite with quartz form due to the breakdown of petalite.

5.2 | Spatial Distribution of Li from LIBS

The average Li content of the spodumene measured from the block samples of the samples was in the range 1.4 to 2.1 wt % Li. In a Li-Si-Al ternary diagram based on the average atomic proportions of these elements within the spodumene crystals (Figure 26), the samples were depleted in Li and enriched in Si compared to literature and the theoretical composition (3.73 wt % Li). The expected range for Li in spodumene at 2.8 to 3.5 wt % Li (Aylmore et al., 2018). This may be caused by the LIBS analyser used not being calibrated to the sample specifically, or be a bias because locations with no measured Li were manually set to zero. The Li content should be checked using another method such as LA-ICP-MS (Rohiman et al., 2023) for true quantitative analysis. The Li content in spodumene in both Sweden and Mali show lower Li concentrations than in other literature for LCT pegmatites but this may be caused by the LIBS system used.

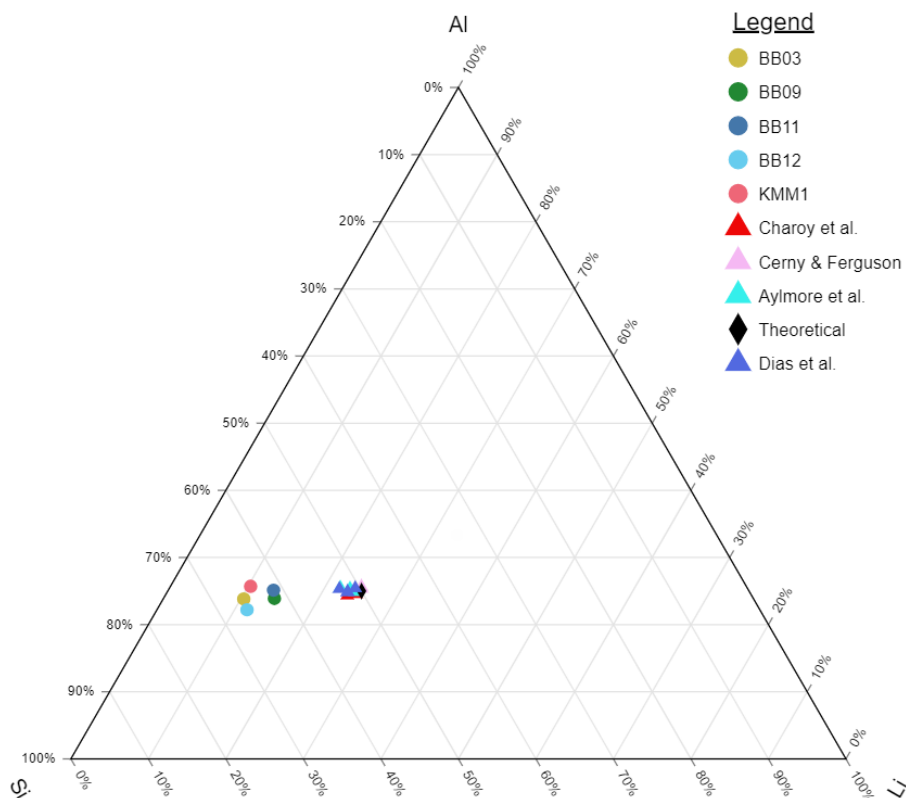


Figure 26. Ternary diagram of Li, Al and Si. The average compositions of spodumene for the samples measured from the block samples are plotted in terms of atomic proportions, along with several examples from literature (Aylmore et al., 2018; Černý & Ferguson, 1972; Charoy et al., 1992; Dias et al., 2023). Ternary plot made using TernaryPlot.com.

The profiles measured from the block sample data showed that the Li content increased sharply at the boundary of the spodumene and feldspar or quartz. The mean Li content throughout the spodumene

crystal is reached within around 80 μm of the boundary. Given the approximately 40 μm spacing between measure points (spot size 10 μm diameter) and the large fluctuations in the Li content throughout the spodumene crystal, it cannot be determined if this increase from the boundary is gradual. Li depletion from the edges of spodumene crystals can be caused by the exchange of material between the spodumene and hydrothermal fluids passing through the pegmatite (Lai et al., 2023). Acke et al. (2023) observed this decrease in Li content at the edges of spodumene crystal also using LIBS but with a spot size of 100 μm . To confirm whether this gradual increase occurs, closer spacing would be needed between the measured points. The majority of the lithium remains contained within the spodumene crystals and is not noticeably depleted at the edges.

In sample BB11, a rim of feldspar intergrown with fine grained feldspar and quartz is present around one edge of the spodumene crystal. LIBS analysis of this area showed greater fluctuations in Li content and a lower average Li concentration than within the spodumene crystal itself. This confirms the petrographic observations that spodumene has recrystallised within the groundmass of finer grained feldspar and quartz crystals. The fluctuations in Li may be caused by the LIBS measurement points being located on the boundaries of the feldspar and fine spodumene crystals. The exact location of the measured points was not visible on the block samples. The rims around the spodumene crystals vary in composition and thickness (< 50 μm to 1000 μm). This result shows that Li is present outside of the primary, type 1 spodumene crystals.

The average Li content of the spodumene crystals measured on the thin sections using the LIBS was about 1 wt % Li lower than for the block samples. This was influenced by the large number of locations where no Li was recorded and were therefore manually set to zero to calculate the averages. Cross plots of Li vs Al and Li vs Si were plotted excluding these zero values. There was a weak to moderate correlation between Li and Al in all samples. This suggests that Li and Al may be affected similarly by processes which determine their concentrations within the spodumene crystal, for example leaching. Li and Al have weaker electrostatic bond strengths than Si in the spodumene crystal structure (Moon & Fuerstenau, 2003) which could make them more susceptible to be leached out of the spodumene crystal. However the dissolution of these ions is also dependent on other aspects of crystal chemistry as well as fluid composition, temperature and pressure. Li and Al correlations in the LIBS data may be caused by the weaker bonds strengths than the Si in the spodumene crystal structure making them more susceptible to leaching.

The cross plots highlight that no measurements recorded a Li content below 0.5 wt % Li. This could be the limit of what can be detected for Li in this type of mineral structure by this laser and set up. However, most LIBS have ppm level Limit of Detection (LOD). For example, Fabre (2020) reported that LIBS analysis was able to measure to 5 ppm Li for spodumene with concentrations of 3.5 ± 0.7 wt % Li. No LOD was provided with the Keyence EA-300. In this case it appears that 0.5 wt % Li is the limit of what can be detected for Li in this type of mineral structure by the Keyence EA-300 LIBS system.

The data collected from the thin sections shows a higher concentration of Li in fractures and cleavage planes in the spodumene than in the surrounding non-fractured spodumene crystal. In many of the measurements within the non-fractured parts of the spodumene mineral, no Li was recorded. The fractures and cleavage planes analysed in the samples were extremely thin (often approx. 10 μm wide) and this result would imply that Li is leached from the spodumene and precipitated in fractures in the mineral. Acke et al. (2023) performed LIBS mapping of Li content in spodumene and found a depletion of Li along fractures and cleavage planes. This difference could be caused by the samples themselves or differences in the LIBS systems used, such as the 10 times larger spot size used by Acke et al. (2023) and different laser characteristics. The higher Li content in the fractures in spodumene than in the crystal may be due to the sample preparation and LIBS system used. This is further discussed in section 5.3.

5.3 | Li Determination with LIBS – Feasible?

LIBS measurements are significantly affected by matrix effects and sample preparation. Matrix effects include physical and chemical properties of the sample that affect the creation of plasma during the analysis (Palleschi, 2020). Factors such as roughness and optical characteristics (transmissivity and reflectivity) of the sample may affect the laser-material coupling (Wise et al., 2022) and could explain why the Li content measured in the thin sections was much lower than in the block samples. The block samples were cut using a diamond rock saw while creating the thin sections so that they are flat surfaces but they were not polished like the thin sections, making their surfaces rougher. Rough surfaces can cause the laser not to be focussed perfectly on the sample surface and may result in less of the sample being ablated by the laser pulse during the measurement. This could cause some measurements to not record Li in the block samples. However, even with a polished surface, less Li is recorded by the LIBS from the thin sections. The polishing of the thin section also causes the section to become more reflective to light, including the laser pulse. Additionally, the sample is extremely thin (30 μm) and has been prepared so that light can pass through it for use in optical microscopy. Either this transmissivity or reflectivity of the laser beam could cause the power of the laser to be decreased, potentially causing less ablation of material so less Li was detected. Harmon et al. (2009) stated that plasmas are more strongly developed on opaque than transparent minerals. Fractures and cleavage planes are visible because they do not transmit light through the sample as much as the surrounding spodumene mineral. This could also be causing more of the sample to be turned into plasma and hence have a higher Li content in the fractures than in the surrounding crystal. The depth of penetration of the laser in the Keyence EA-300 is typically between 4 and 7 μm and it should therefore not have passed through the entire thickness of the thin section (30 μm). The results of the LIBS analysis highlight that measures should be taken to reduce physical matrix effects of the samples and that thin sections may not be suitable for LIBS analysis due to reflectance and transmission of the laser pulse potentially causing less plasma formation.

The wavelength of the laser used in LIBS measurements can also have an effect on the element concentrations measured. The Keyence EA-300 uses a 355 nm laser, contrary to other studies which used 1064 nm wavelength laser when using LIBS to measure Li in pegmatites (Dias et al., 2023; Fabre et al., 2022; Wise et al., 2022). Advantages of using a shorter wavelength laser for LIBS analysis is that it often has better laser-material coupling and spectral resolution (Senesi, 2014) and is a better option for materials with a high evaporation threshold like rock samples (Fantoni et al., 2006). Cui et al. (2020) showed that self-absorption during the LIBS measurement is greater for 355 nm lasers than 1064 nm laser which would decrease the intensity of the peaks recorded by the spectrometer. The wavelength of the laser in the LIBS has effects on plasma generation and self-absorption and should be noted when comparing the results of this study with other literature.

The data provided by the Keyence EA-300 is given in wt % however this data should not be assumed to be quantitative. The intensities of the peaks recorded by the spectrometer are converted into amounts of each element by calibration curves. In this case, calibration curves were provided with the elemental analyser and these were therefore not specific for spodumene in pegmatites. This again relates to matrix effects of the sample as the amount of ions that are ablated is dependent on the structure of the material, in this case the mineral structure (Harmon et al., 2019). In an ideal case, a calibration curve would be created from a rock of similar composition but with a known elemental composition (Palleschi, 2020). This would allow the LOD to be determined for each element (Palleschi, 2022). As this was not possible for this study, the data should be viewed as qualitative or semi-quantitative.

In addition to uncertainties concerning the LIBS analysis and the analyser itself, there are errors in handling the analyser and how and where measurements were taken. There was uncertainty in the determining exact location of mineral boundaries as the minimum viewing magnification of the

Keyence EA-300 elemental analyser is 300 times. The boundaries between minerals will also give mixed signals in the spectra (Müller & Meima, 2022). The measurement points may also not be perfectly placed on specific structures such as boundaries or fractures within the mineral. The locations of the profiles taken are chosen by the user so this invokes some element of bias in the resulting data. Introducing a capability to map an entire section of a sample using a random or pre-determined grid would improve the quality of data collected and allow maps of the Li content across entire spodumene crystals to be made. The exact locations of boundaries or fractures with respect to the measured points is not known precisely and the small spot size means some features may be missed in the LIBS profiles.

6 | Conclusion

The aim of this study was to investigate the distribution of Li in spodumene crystals within Li pegmatites based on samples from LCT pegmatite fields in Sweden and Mali. This was carried out through mineralogical and textural observations from thin section analysis and LIBS analysis using the Keyence EA-300 elemental analyser. Petrographic descriptions were made for each sample and the LIBS data was analysed in profiles in spodumene crystals and by bulk analysis of all data collected from the spodumene crystals.

The following conclusions could be made:

1. The Li remains mostly contained within the spodumene crystals and Li content increases sharply at the spodumene crystal boundary.
2. The Bergby (Sweden) samples show secondary, recrystallised, fine grained spodumene, often in needle-like shapes, around the edges of the primary spodumene crystals and within the fine grained groundmass surrounding it. This causes some patches of lower concentrations of Li to be found outside of the main spodumene crystals in the Bergby (Sweden) samples.
3. Using the Keyence EA-300, the average lithium concentrations measured in spodumene crystals in the thin sections are significantly lower than in the block samples. The thin section LIBS data showed that Li was more often recorded on fractures or cleavage planes within the spodumene crystals, particularly in the Bougouni (Mali) samples. This could be due to sample preparation effects which cause increased reflectivity and transmissivity of the laser on the thin section compared to the block samples.
4. This LIBS system does not provide a quick and inexpensive method to *quantitatively map* the distribution of Li in pegmatites. This would require calibration curves to be made from pegmatite standards and appropriate preparation of the samples. Finding standards would be complicated given the large amount of heterogeneity in pegmatites.

In summary, this study confirmed that Li is mainly contained within spodumene in LCT pegmatites but that secondary recrystallisation of spodumene does occur in the surrounding groundmass. The Keyence EA-300 is not an appropriate method for quantitative analysis but the LIBS technique in general has good potential for mapping Li in LCT pegmatites.

7 | Outlook & Recommendations

Li is classified as a critical raw material which means that it is of high economic importance, has a high supply risk and lacks viable substitutes. This makes the exploration and recovery of Li important, particularly for the energy transition if the current goals are to be met. This study has confirmed findings by other authors (e.g. Acke et al., 2023) that Li is not solely contained within the coarse spodumene crystals but also in finer grained material in surrounding groundmass and intergrown with other minerals with symplectic texture. In future it may be possible to relate these textures to specific zones in pegmatites or particular events in the pegmatites' geologic histories. In further studies it would be important to assess whether Li can be recovered efficiently from these additional Li-bearing components in the pegmatites as methods like flotation currently have poor recovery of fine spodumene crystals. The edges of the spodumene and fractures in the crystals have been shown by other literature to be depleted in Li so quantitative analysis on samples where fractures are clearly visible without needing to make thin sections would be needed to confirm this. This could be developed further into determining what controls these processes and what it could mean for Li recovery from LCT pegmatites. The fast and accurate generation of calibration curves for LIBS analysis is already an active area of research (e.g. Fabre et al., 2022) but it is particularly relevant for quantitatively measuring Li as few other techniques can detect Li. Methods such as XRD or ICP-MS are alternatives for Li detection. The sensitivity and LOD of the Keyence EA-300 elemental analyser would be important to investigate and determine whether this LIBS set up can be adapted to make it more suitable for identifying Li in spodumene crystals in pegmatites.

Supplementary Data

Supplementary data from this study are available via the TU Delft Bachelor Thesis online repository or through my supervisors (T. Schmiedel and F. Desta). This includes: the entire thin section scans from the Zeiss Axioscan, the raw data as it was exported from the Keyence EA-300 and the excel files containing the data as it was used in this report (labelled in accordance with the figures in the appendix).

References

- Acke, J., 1,4, Kwizera, D., Goodship, A., Dewaele, S., 4, Consortium for Battery Innovation, Royal Belgian Institute of Natural Sciences, University of Liège, & Borst, A., 1,2. (2023). Spodumene textural variations in a deformed LCT-type pegmatite. A case study from the Musha-Ntungwa area, Rwanda. In *Conference Paper*.
- Aylmore, M. G., Merigot, K., Rickard, W. D., Evans, N. J., McDonald, B. J., Catovic, E., & Spitalny, P. (2018). Assessment of a spodumene ore by advanced analytical and mass spectrometry techniques to determine its amenability to processing for the extraction of Li. *Minerals Engineering*, 119, 137–148. <https://doi.org/10.1016/j.mineng.2018.01.010>
- Bischoff, I., & Bischoff, A. A. (1988). A Li-bearing pegmatite from the Vredefort Dome. *South African Journal of Geology*, 91(4), 550–552. <https://pubs.geoscienceworld.org/gssa/sajg/article-abstract/91/4/550/122162/A-Li-bearing-pegmatite-from-the-Vredefort>
- Bougouni Li Project, Bamako, Southern Mali, West Africa*. (2020, February 28). NS Energy. <https://www.nsenergybusiness.com/projects/bougouni-Li-project/?cf-view>
- Bradley, D. C., Stillings, L. L., Jaskula, B. W., Munk, L., & McCauley, A. D. (2017). Lithium. U.S. Geological Survey Professional Papers/U.S. Geological Survey Professional Paper. <https://doi.org/10.3133/pp1802k>
- Breaks, F., Selway, J. B., & Tindle, A. (2003). *Fertile peraluminous granites and related rare-element mineralization in pegmatites, Superior Province, northwest and northeast Ontario : Operation Treasure Hunt*. <https://www.semanticscholar.org/paper/Fertile-peraluminous-granites-and-related-in-and--Breaks-Selway/acf306ec7d59e9f4571239f9dc98cd2c324c8ca6>
- British Geological Survey. (2021). *Li: a critical raw material for our journey to net zero*. <https://www.bgs.ac.uk/news/Li-a-critical-raw-material-for-our-journey-to-net-zero/>
- Cerny, P., & Ferguson, R. B. (1972). The Tanco pegmatite at Bernic Lake, Manitoba; IV, Petalite and spodumene relations. *Canadian Mineralogist*, 11(3), 660–678. <https://pubs.geoscienceworld.org/canmin/article/11/3/660/10862/The-Tanco-pegmatite-at-Bernic-Lake-Manitoba-IV>
- Černý, P., & London, D. (1983). Crystal chemistry and stability of petalite. *TMPM. Tschermaks Mineralogische Und Petrographische Mitteilungen*, 31(1–2), 81–96. <https://doi.org/10.1007/bf01084763>
- Charoy, B., Lhote, F., Dusausoy, Y., & Noronha, F. (1992). The crystal chemistry of spodumene in some granitic aplite-pegmatite bodies of northern Portugal; a comparative review. *Canadian Mineralogist*, 30(3), 639–651. <https://pubs.geoscienceworld.org/canmin/article-abstract/30/3/639/12381/The-crystal-chemistry-of-spodumene-in-some>

- Charoy, B., Noronha, F., & Lima, A. (2001). SPODUMENE PETALITE EUCRYPTITE: MUTUAL RELATIONSHIPS AND PATTERN OF ALTERATION IN Li-RICH APLITE PEGMATITE DYKES FROM NORTHERN PORTUGAL. *Canadian Mineralogist*, 39(3), 729–746. <https://doi.org/10.2113/gscanmin.39.3.729>
- Chen, J., Zhang, H., Tang, Y., Lv, Z., An, Y., Wang, M., Liu, K., & Xu, Y. (2022). Li mineralization during evolution of a magmatic–hydrothermal system: Mineralogical evidence from Li-mineralized pegmatites in Altai, NW China. *Ore Geology Reviews*, 149, 105058. <https://doi.org/10.1016/j.oregeorev.2022.105058>
- Critical raw materials*. (n.d.). Internal Market, Industry, Entrepreneurship and SMEs. https://single-market-economy.ec.europa.eu/sectors/raw-materials/areas-specific-interest/critical-raw-materials_en
- Dias, F., Ribeiro, R., Gonçalves, F., Lima, A., Roda-Robles, E., & Martins, T. (2023). Calibrating a Handheld LIBS for Li Exploration in the Barroso–Alvão Aplite-Pegmatite Field, Northern Portugal: Textural Precautions and Procedures When Analyzing Spodumene and Petalite. *Minerals*, 13(4), 470. <https://doi.org/10.3390/min13040470>
- Elemental Analysis with Digital Microscopes Using LIBS (Laser Induced Breakdown Spectroscopy) / KEYENCE America*. (n.d.). <https://www.keyence.com/products/microscope/digital-microscope/industries/other/libs.jsp>
- Element-to-stoichiometric oxide conversion factors*. (2022, August 24). James Cook University. <https://www.jcu.edu.au/advanced-analytical-centre/resources/element-to-stoichiometric-oxide-conversion-factors>
- Fabre, C. (2020). Advances in Laser-Induced Breakdown Spectroscopy analysis for geology: A critical review. *Spectrochimica Acta. Part B, Atomic Spectroscopy*, 166, 105799. <https://doi.org/10.1016/j.sab.2020.105799>
- Fabre, C., Ourti, N. E., Ballouard, C., Mercadier, J., & Cauzid, J. (2022). Handheld LIBS analysis for in situ quantification of Li and detection of the trace elements (Be, Rb and Cs). *Journal of Geochemical Exploration*, 236, 106979. <https://doi.org/10.1016/j.gexplo.2022.106979>
- Feng, Y., Liang, T., Yang, X., Zhang, Z., & Wang, Y. (2019). Chemical Evolution of Nb-Ta Oxides and Cassiterite in Phosphorus-Rich Albite-Spodumene Pegmatites in the Kangxiwa–Dahongliutan Pegmatite Field, Western Kunlun Orogen, China. *Minerals*, 9(3), 166. <https://doi.org/10.3390/min9030166>
- Harmon, R. S., Lawley, C. J., Watts, J., Harraden, C. L., Somers, A. M., & Hark, R. R. (2019). Laser-Induced Breakdown Spectroscopy—An Emerging Analytical Tool for Mineral Exploration. *Minerals*, 9(12), 718. <https://doi.org/10.3390/min9120718>
- Högdahl, K., Jonsson, E., Leijed, M., & Bergqvist, M. (2024). The Bergby LCT-type granitic pegmatite field in the Ljusdal lithotectonic unit, central Sweden. *ResearchGate*.

- https://www.researchgate.net/publication/378183264_The_Bergby_LCT-type_granitic_pegmatite_field_in_the_Ljusdal_lithotectonic_unit_central_Sweden
- Högdahl, K., Jonsson, E., Leijd, M., & Kördel, M. (2023). The Bergby LCT-pegmatite Field, Central Sweden -A New Contender to Produce Swedish Lithium? SEG 2023. . . ResearchGate. https://www.researchgate.net/publication/378183098_The_Bergby_LCT-pegmatite_Field_Central_Sweden_-_A_New_Contender_to_Produce_Swedish_Lithium_SEG_2023_Conference_Resourcing_the_Green_Transition
- Högdahl, K., Sjöström, H., & Bergman, S. (2009). Ductile shear zones related to crustal shortening and domain boundary evolution in the central Fennoscandian Shield. *Tectonics*, 28(1). <https://doi.org/10.1029/2008tc002277>
- Holzer, A., Zimmermann, J., Wiszniewski, L., Necke, T., Gatschlhofer, C., Öfner, W., & Raupenstrauch, H. (2022). A Combined Hydro-Mechanical and Pyrometallurgical Recycling Approach to Recover Valuable Metals from Li-Ion Batteries Avoiding Li Slagging. *Batteries*, 9(1), 15. <https://doi.org/10.3390/batteries9010015>
- IEA. (2021). *The Role of Critical Minerals in Clean Energy Transitions – Analysis - IEA*. <https://www.iea.org/reports/the-role-of-critical-minerals-in-clean-energy-transitions/executive-summary>
- IEA. (2023, July 11). *Critical minerals market sees unprecedented growth as clean energy demand drives strong increase in investment - News - IEA*. <https://www.iea.org/news/critical-minerals-market-sees-unprecedented-growth-as-clean-energy-demand-drives-strong-increase-in-investment>
- KEYENCE CORPORATION. (2024). Laserbasierte Materialanalyse-Einheit Modellreihe EA-300.
- Koopmans, L., Martins, T., Linnen, R., Gardiner, N. J., Breasley, C. M., Palin, R. M., Groat, L. A., Silva, D., & Robb, L. J. (2023). The formation of Li-rich pegmatites through multi-stage melting. *Geology*, 52(1), 7–11. <https://doi.org/10.1130/g51633.1>
- Kusky, W. D., Jr., Mooney, W. D., Windley, B. F., Cawood, P. A., Kröner, A., Collins, W. J., Kusky, T. M., & Windley, B. F. (2009). Accretionary orogens through Earth history. *Geological Society, London, Special Publications*, 318, 1–36. <https://doi.org/10.1144/SP318.1>
- Lai, X., Chen, C., Chen, X., Fei, G., Li, Y., Wang, J., & Cai, Y. (2023). Process Mineralogy Characteristics of Lijiagou Pegmatite Spodumene Deposit, Sichuan, China. *Minerals*, 13(9), 1180. <https://doi.org/10.3390/min13091180>
- Leijd, M., Högdahl, K., Jonsson, E., & Zetterqvist, A. (2023). FIELD TRIP GUIDE. In GREENPEG International Conference, *The Bergby LCT-pegmatite Field in the Hamrånge Area*. <https://www.greenpeg.eu/>

- Lima, A., & Dias, F. (2019). Spodumene and Quartz intergrowth - textural and genesis point of view. *EGU General Assembly Conference Abstracts*, 13404.
<https://ui.adsabs.harvard.edu/abs/2019EGUGA..2113404L/abstract>
- London, D. (2014). A petrologic assessment of internal zonation in granitic pegmatites. *Lithos*, 184–187, 74–104. <https://doi.org/10.1016/j.lithos.2013.10.025>
- London, D. (2018). Ore-forming processes within granitic pegmatites. *Ore Geology Reviews*, 101, 349–383. <https://doi.org/10.1016/j.oregeorev.2018.04.020>
- London, D., & Burt, D. M. (1982, February 1). *Alteration of spodumene, montebrasite and lithiophilite in pegmatites of the White Picacho District, Arizona*. *American Mineralogist* | GeoScienceWorld. <https://pubs.geoscienceworld.org/msa/ammin/article-abstract/67/1-2/97/104783/Alteration-of-spodumene-montebrasite-and>
- Mackenzie, W., & Guilford, C. (2014). *Atlas of the Rock-Forming minerals in thin section*. Routledge.
- MacKenzie, W. S., Donaldson, C., & Guilford, C. (1983). *Atlas of igneous rocks and their textures*. <https://www.semanticscholar.org/paper/Atlas-of-igneous-rocks-and-their-textures-MacKenzie-Donaldson/f25a0db44a0512e63a996985175c0951dbd214b7>
- Moon, K. S., & Fuerstenau, D. W. (2003). Surface crystal chemistry in selective flotation of spodumene (LiAl[SiO₃]₂) from other aluminosilicates. *International Journal of Mineral Processing*, 72(1–4), 11–24. [https://doi.org/10.1016/s0301-7516\(03\)00084-x](https://doi.org/10.1016/s0301-7516(03)00084-x)
- Müller, A., Simmons, W., Beurlen, H., Thomas, R., Ihlen, P. M., Wise, M., Roda-Robles, E., Neiva, A. M., & Zagorsky, V. (2018). A proposed new mineralogical classification system for granitic pegmatites – Part I: History and the need for a new classification. *Canadian Mineralogist*, 60(2), 203–227. <https://doi.org/10.3749/canmin.1700088>
- Müller, S., & Meima, J. A. (2022). Mineral classification of Li-bearing pegmatites based on laser-induced breakdown spectroscopy: Application of semi-supervised learning to detect known minerals and unknown material. *Spectrochimica Acta. Part B, Atomic Spectroscopy*, 189, 106370. <https://doi.org/10.1016/j.sab.2022.106370>
- Ogenhall, E. (2010). Geological Evolution of the Supracrustal Palaeoproterozoic Hamrånge Group: A Svecofennian Case Study. DIVA. <https://uu.diva-portal.org/smash/record.jsf?pid=diva2%3A310075&dswid=-7263>
- Ogenhall, E., Sjöström, H., Andersson, U., & Högdahl, K. (2010). The geology of the Hamrånge area, a summary of the tectonothermal evolution in the west-central part of the Fennoscandian Shield. In NGF No. 1, Abstracts and proceedings of the Geological Survey of Norway, 29th Nordic Geological Wintermeeting, Oslo (pp. 138–139). <http://www.diva-portal.org/smash/record.jsf?pid=diva2:928285>
- Okrusch, M., & Frimmel, H. E. (2020). Pegmatites. In *Springer textbooks in earth sciences, geology and environment* (pp. 371–377). https://doi.org/10.1007/978-3-662-57316-7_22

- Palleschi, V. (2020). Laser-induced breakdown spectroscopy: principles of the technique and future trends. *ChemTexts*, 6(2). <https://doi.org/10.1007/s40828-020-00114-x>
- Palleschi, V. (2022, December 2). Avoiding Misunderstanding Self-Absorption in Laser-Induced Breakdown Spectroscopy (LIBS) Analysis. *Spectroscopy Online*. <https://www.spectroscopyonline.com/view/avoiding-misunderstanding-self-absorption-in-laser-induced-breakdown-spectroscopy-lib-s-analysis>
- pearsonr — SciPy v1.14.0 Manual. (n.d.). <https://docs.scipy.org/doc/scipy/reference/generated/scipy.stats.pearsonr.html>
- Phelps, P. R., Lee, C. A., & Morton, D. M. (2020). Episodes of fast crystal growth in pegmatites. *Nature Communications*, 11(1). <https://doi.org/10.1038/s41467-020-18806-w>
- Plas, L. V. D., & Tobi, A. C. (1965). A chart for judging the reliability of point counting results. *American Journal of Science* / the α American Journal of Science, 263(1), 87–90. <https://doi.org/10.2475/ajs.263.1.87>
- Rai, V., & Thakur, S. N. (2020). Physics and dynamics of plasma in laser-induced breakdown spectroscopy. In *Elsevier eBooks* (pp. 71–106). <https://doi.org/10.1016/b978-0-12-818829-3.00004-6>
- Rohiman, A., Setiyanto, H., Saraswaty, V., & Amran, M. B. (2023). Review of analytical techniques for the determination of Li: From conventional to modern technique. ResearchGate. <https://doi.org/10.48317/IMIST.PRSM/morjchem-v11i04.40229>
- Sanogo, S., Durand, C., Dubois, M., & Wane, O. (2021). *Structural constraints of the birimian Li pegmatites of Bougouni (Southern Mali, Leo-Man Shield)*. <https://doi.org/10.5194/egusphere-egu21-6752>
- Senesi, G. S., & De Pascale, O. (2022). Laser-Induced Breakdown Spectroscopy (LIBS) In-Situ: From Portable to Handheld Instrumentation. In *Springer eBooks* (pp. 465–503). https://doi.org/10.1007/978-3-030-60016-7_17
- Simmons, W. B. S., & Webber, K. L. (2008). Pegmatite genesis: state of the art. *European Journal of Mineralogy*, 20(4), 421–438. <https://doi.org/10.1127/0935-1221/2008/0020-1833>
- Swain, B. (2017). Recovery and recycling of Li: A review. *Separation and Purification Technology*, 172, 388–403. <https://doi.org/10.1016/j.seppur.2016.08.031>
- Sweetapple, M. T., & Tassios, S. (2015). Laser-induced breakdown spectroscopy (LIBS) as a tool for in situ mapping and textural interpretation of Li in pegmatite minerals. *the α American Mineralogist*, 100(10), 2141–2151. <https://doi.org/10.2138/am-2015-5165>
- Szentpéteri, K., Cutts, K., Glorie, S., O'Brien, H., Lukkari, S., Radoslaw, M. M., & Butcher, A. (2024). First in situ Lu–Hf garnet date for a Li–caesium–tantalum (LCT) pegmatite from the Kietyönmäki Li deposit, Somero–Tammela pegmatite region, SW Finland. *European Journal of Mineralogy*, 36(3), 433–448. <https://doi.org/10.5194/ejm-36-433-2024>

- Szlugaj, J., Radwanek-Bąk, B., & Mineral and Energy Economy Research Institute, Polish Academy of Sciences, Kraków, Poland. (2022). Li sources and their current use. In *Gospodarka Surowcami Mineralnymi – Mineral Resources Management* (Vols. 38–38, Issue 1, pp. 61–88). <https://doi.org/10.24425/gsm.2022.140613>
- Thomas, R., Bühmann, D., Bullen, W., Scogings, A., & De Bruin, D. (1994). Unusual spodumene pegmatites from the Late Kibaran of southern Natal, South Africa. *Ore Geology Reviews*, 9(2), 161–182. [https://doi.org/10.1016/0169-1368\(94\)90026-4](https://doi.org/10.1016/0169-1368(94)90026-4)
- Thomas, R., Webster, J. D., & Davidson, P. (2006). Understanding pegmatite formation: The melt and fluid inclusion approach. *ResearchGate*.
https://www.researchgate.net/publication/236882856_Understanding_pegmatite_formation_The_melt_and_fluid_inclusion_approach
- Wang, Z., Li, J., Chen, Z., Yan, Q., Xiong, X., Li, P., & Deng, J. (2021). Evolution and Li Mineralization of the No. 134 Pegmatite in the Jijika Rare-Metal Deposit, Western Sichuan, China: Constrains from Critical Minerals. *Minerals*, 12(1), 45.
<https://doi.org/10.3390/min12010045>
- Warr, L. N. (2021). IMA–CNMNC approved mineral symbols. *Mineralogical Magazine*, 85, 291–320. <https://doi.org/10.1180/mgm.2021.43>
- West African Exploration Initiative (WAXI). (n.d.). Geological Background Map.
- Wilde, A., Otto, A., & McCracken, S. (2021). Geology of the Goulamina spodumene pegmatite field, Mali. *Ore Geology Reviews*, 134, 104162. <https://doi.org/10.1016/j.oregeorev.2021.104162>
- Wise, M. A., Harmon, R. S., Curry, A., Jennings, M., Grimac, Z., & Khashchevskaya, D. (2022). Handheld LIBS for Li Exploration: An Example from the Carolina Tin-Spodumene Belt, USA. *Minerals*, 12(1), 77. <https://doi.org/10.3390/min12010077>
- Xie, R., Zhu, Y., Liu, J., Li, Y., Wang, X., & Shumin, Z. (2020). Research Status of spodumene flotation: A review. *Mineral Processing and Extractive Metallurgy Review*, 42(5), 321–334. <https://doi.org/10.1080/08827508.2020.1776278>

Appendix

Appendix A: Image of the Block Samples

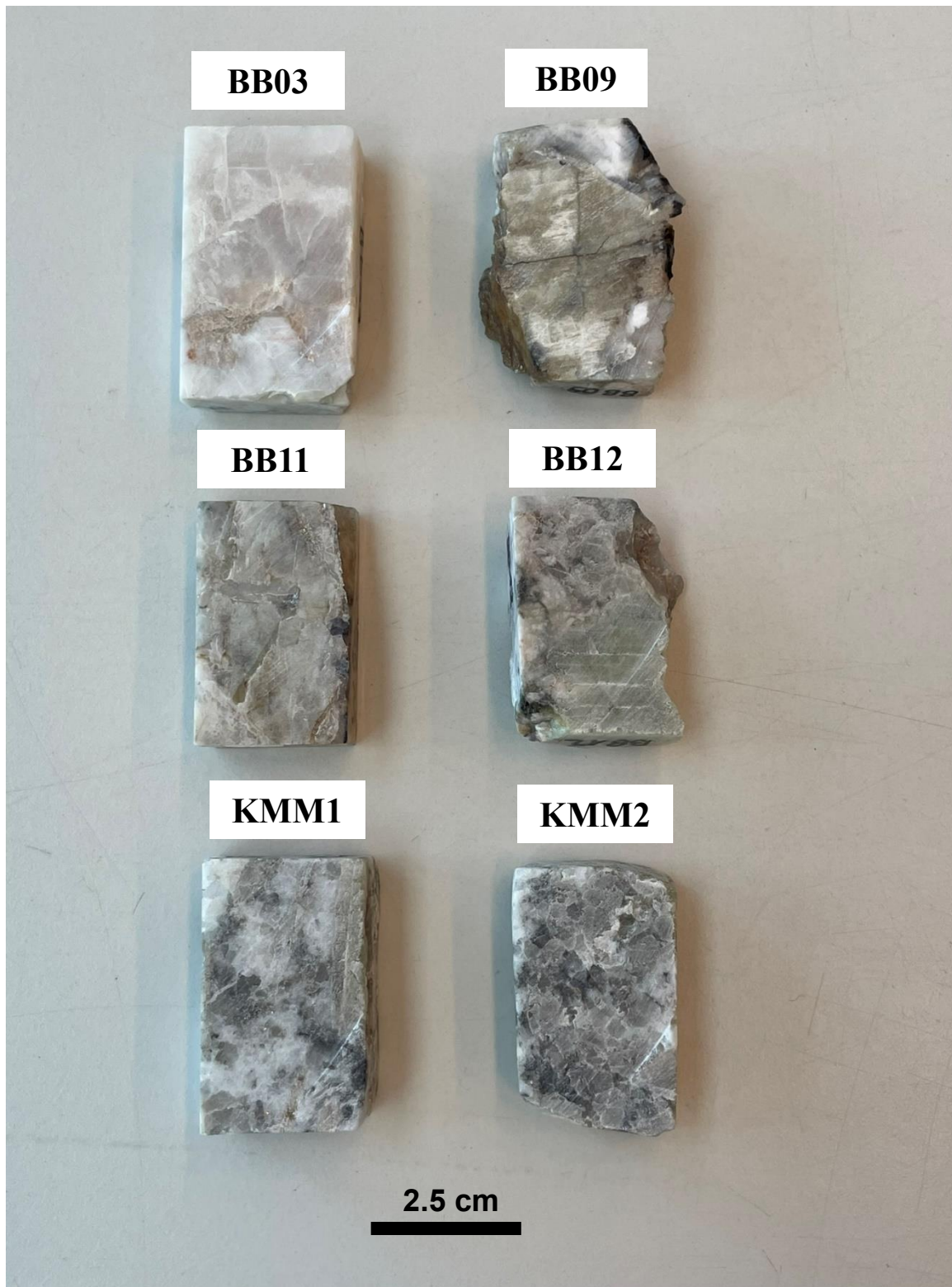


Figure A1. The block samples corresponding to the thin sections for each sample.

Appendix B: Spectra for main minerals

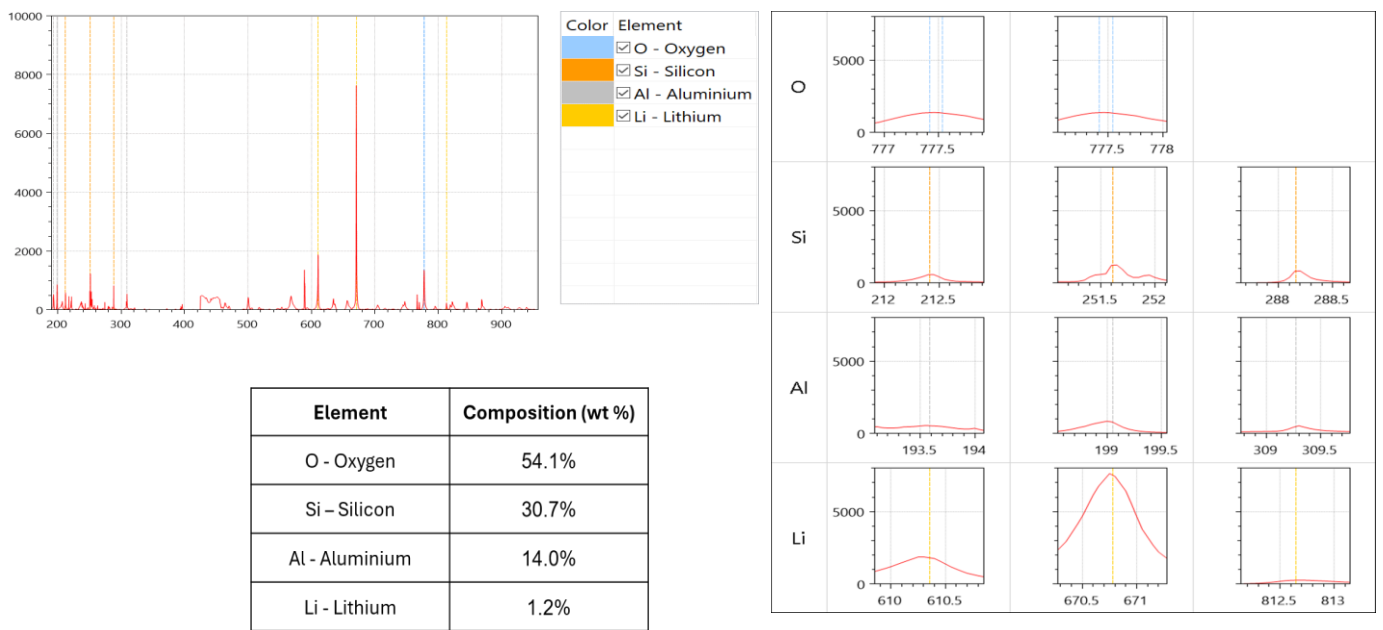


Figure B1. The spectrum for Spodumene, a zoomed in view of the peaks and the elemental analysis provided for the point measured.

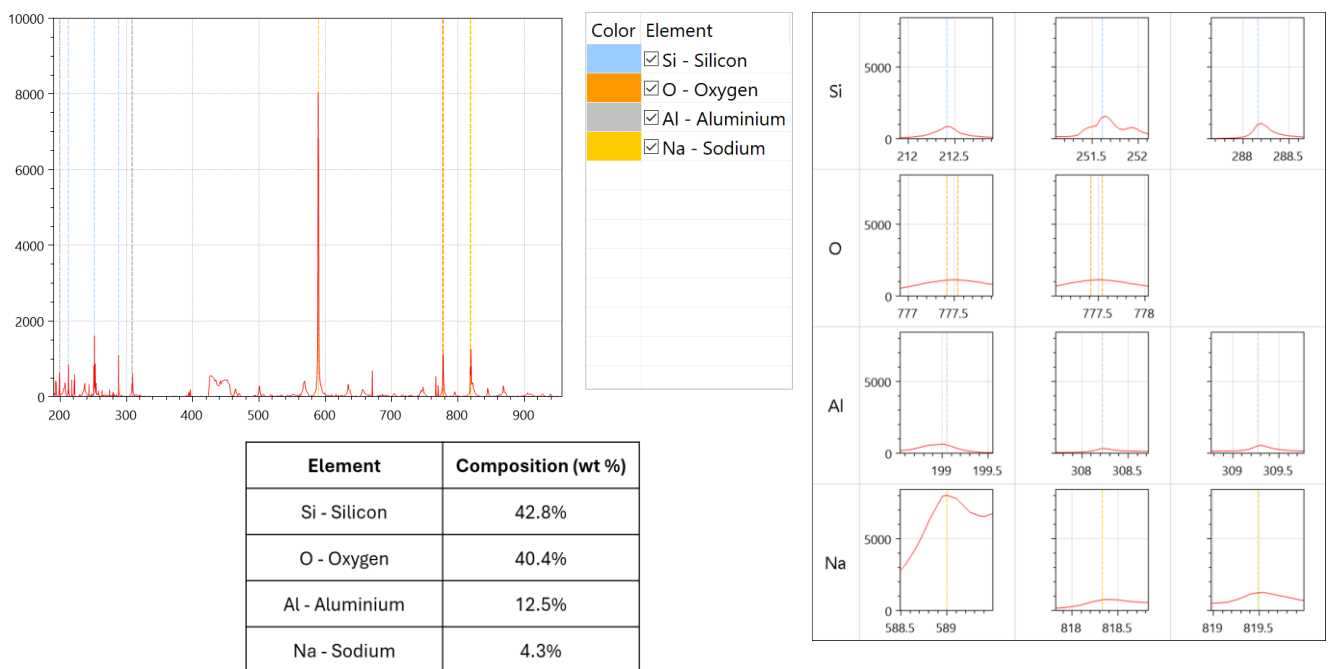
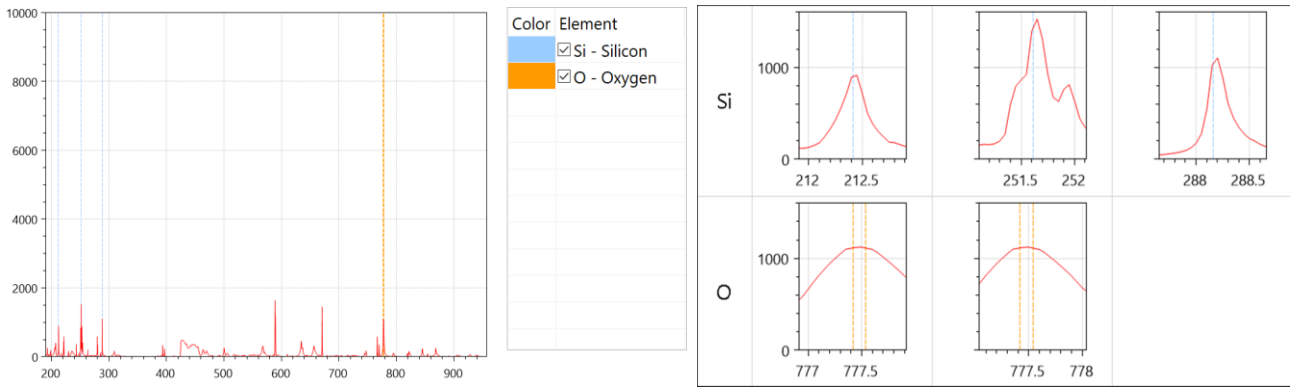


Figure B2. The spectrum for feldspar, a zoomed in view of the peaks and the elemental analysis provided for the point measured.



Element	Composition (wt %)
Si - Silicon	59.9%
O - Oxygen	40.1%

Figure B3. The spectrum for quartz, a zoomed in view of the peaks and the elemental analysis provided for the point measured.

Appendix C: LIBS Average Compositions

Table C1. The average elemental composition of each sample measured from the block samples.

	Si	O	Al	Li	Na	K	Au	Ag	Cu	H	C	Fe	P
BB03	39.37	45.40	13.69	1.54	-	-	-	-	-	-	-	-	-
BB09	36.48	44.51	13.56	2.09	0.56	2.44	0.18	0.04	0.01	0.11	0.0	0.37	-
BB11	38.17	44.02	15.03	2.09	0.13	0.57	-	-	-	-	-	-	-
BB12	41.31	41.03	13.32	1.79	0.62	1.88	-	-	-	-	-	-	0.05
KMM1	35.39	48.97	13.66	1.42	0.01	0.01	-	-	-	0.03	0.44	0.05	-
KMM2	-	-	-	-	-	-	-	-	-	-	-	-	-

Table C2. The standard deviation of the elemental composition of each sample measured from the block samples.

	Si	O	Al	Li	Na	K	Au	Ag	Cu	H	C	Fe	P
BB03	3.29	5.38	2.12	0.48	-	-	-	-	-	-	-	-	-
BB09	7.30	8.70	4.25	1.22	1.00	2.66	3.24	0.73	0.24	0.77	0.00	2.34	-
BB11	4.46	4.52	2.54	0.83	0.34	1.58	-	-	-	-	-	-	-
BB12	6.38	4.35	3.84	0.93	0.73	1.44	-	-	-	-	-	-	0.25
KMM1	6.27	8.74	3.37	1.00	0.12	0.12	-	-	-	0.36	5.31	0.65	-
KMM2	-	-	-	-	-	-	-	-	-	-	-	-	-

Table C3. The average elemental composition of each sample measured from the thin sections.

	Si	O	Al	Li	Na	K	Fe
BB03	40.45	46.84	11.70	0.98	0.08	-	-
BB09	38.50	45.87	13.11	1.06	0.19	1.57	0.27
BB11	-	-	-	-	-	-	-
BB12	40.00	46.85	12.04	0.62	0.25	0.14	0.19
KMM1	37.72	50.82	10.88	0.42	0.00	1.03	1.00
KMM2	35.70	53.33	10.33	0.61	0.00	0.00	0.29

Table C4. The standard deviation of the elemental composition of each sample measured from the thin sections.

	Si	O	Al	Li	Na	K	Fe
BB03	5.45	6.52	2.11	0.78	0.26	-	-
BB09	4.80	5.88	3.47	0.86	0.55	2.17	1.51
BB11	-	-	-	-	-	-	-
BB12	5.18	7.35	2.45	0.67	0.37	0.38	0.94
KMM1	5.84	6.83	2.82	0.71	0.07	1.63	3.70
KMM2	8.61	10.99	4.19	0.86	0.00	0.00	1.30

Table C5. The average composition of the unknown mineral in sample BB03. Measured from the thin sections using LIBS analysis.

Si	O	Al	Li
51.08%	41.52%	6.59%	0.81%

Table C6. Statistics on the Al content and Li content inside and outside of the fractures or cleavage planes in the spodumene crystals for all samples combined. Includes points within spodumene crystals where no Li detected which were manually set to zero wt % Li.

	Li in Fractures	Al in Fractures	Li in Crystal	Al in Crystal
Median	1.2	13.0	0.0	10.5
Mean	1.0	12.9	0.4	10.6
Minimum	0.0	0.0	0.0	0.0
Maximum	4.3	20.7	2.9	19.7
Standard Deviation	0.9	3.2	0.7	2.9

Table C7. Statistics on the Al content and Li content inside and outside of the fractures or cleavage planes in the spodumene crystals for all samples combined. Does not include values within spodumene crystals where no Li detected.

	Li in Fractures	Al in Fractures	Li in Crystal	Al in Crystal
Median	1.5	14.0	1.3	13.4
Mean	1.6	14.5	1.4	13.6
Minimum	0.7	9.4	0.8	7.7
Maximum	4.3	20.7	2.9	19.7
Standard Deviation	0.54	2.2	0.4	1.8

Appendix D: Additional examples of LIBS profiles through fractures using thin sections

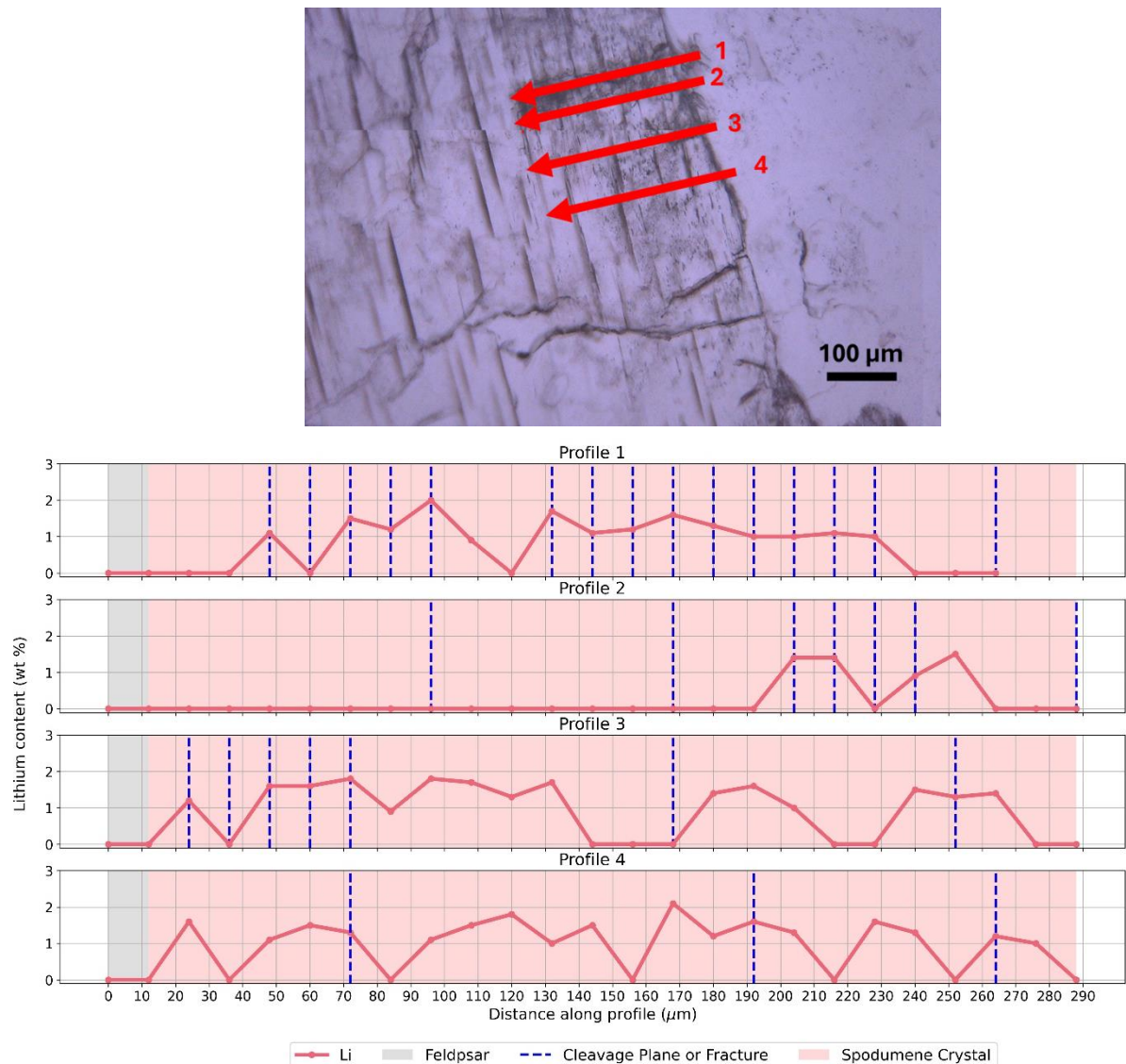
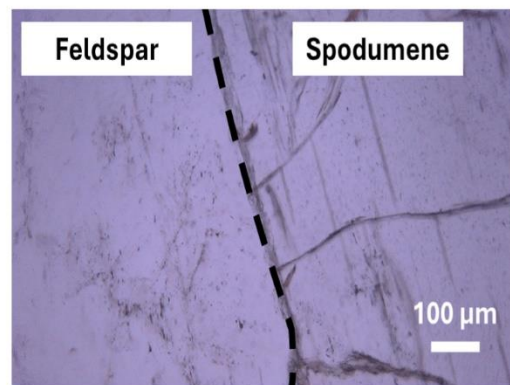
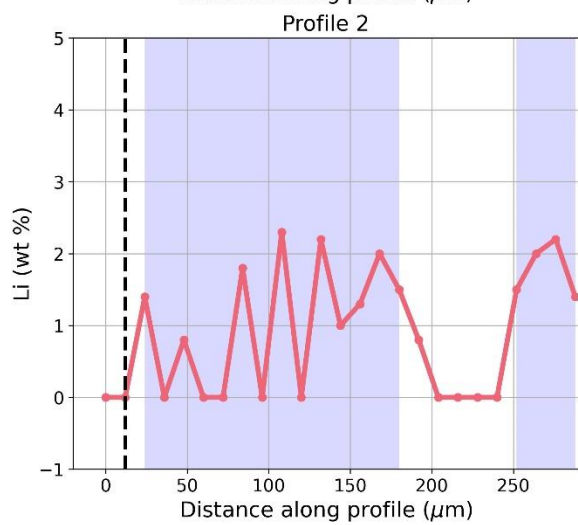
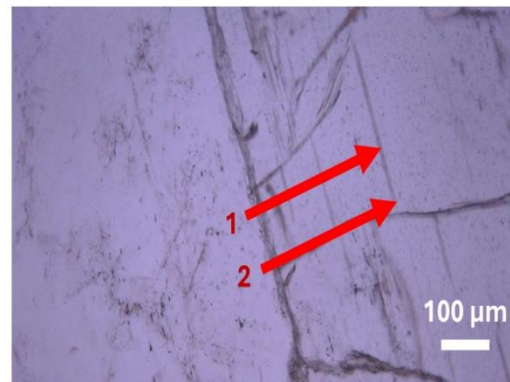
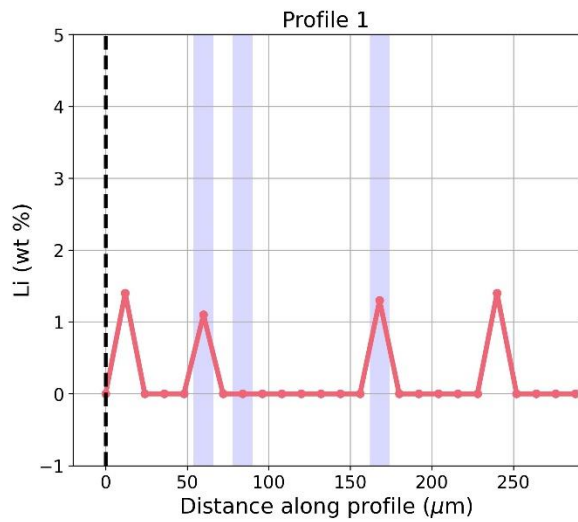


Figure D1. Four parallel profiles showing the Li content across the boundary and into a spodumene crystal in sample KMM1. The locations of the profiles are shown in the above image. The fractures and cleavage planes crossed throughout each profile are indicated.



--- Spodumene Boundary In Fracture

Figure D2. Two profiles showing the Li content taken over different fractures in sample KMM1. The locations of each profile can be seen in the images on the right and the fracture locations on the profiles are marked in blue. The profiles begin on the boundary of a feldspar and spodumene crystal (black dashed line), with measurements taken primarily within the spodumene crystal.

Appendix E: All LIBS profiles for the Block Samples

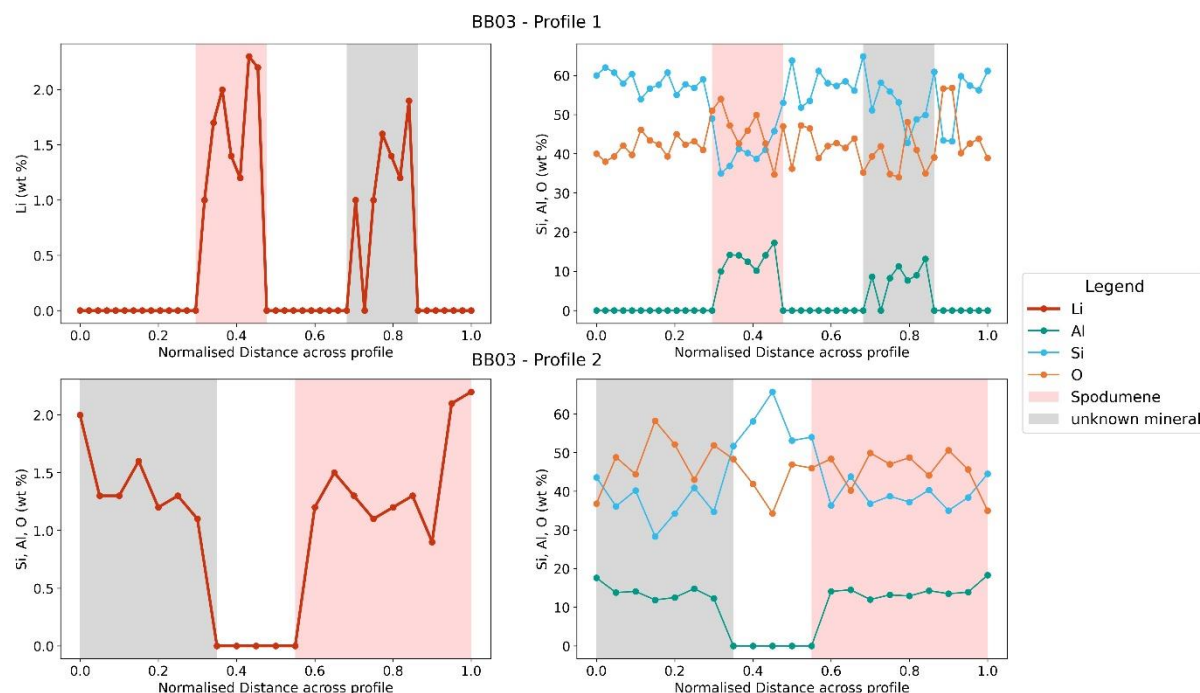


Figure E1. The entire profiles for sample BB03 from the block sample. Li, Al, Si and O wt % is plotted against the normalised distances for each profile. The points recorded in the spodumene crystal are within the red shaded areas. The grey shaded area indicate the unknown mineral, as referred to in the petrographic description for BB03.

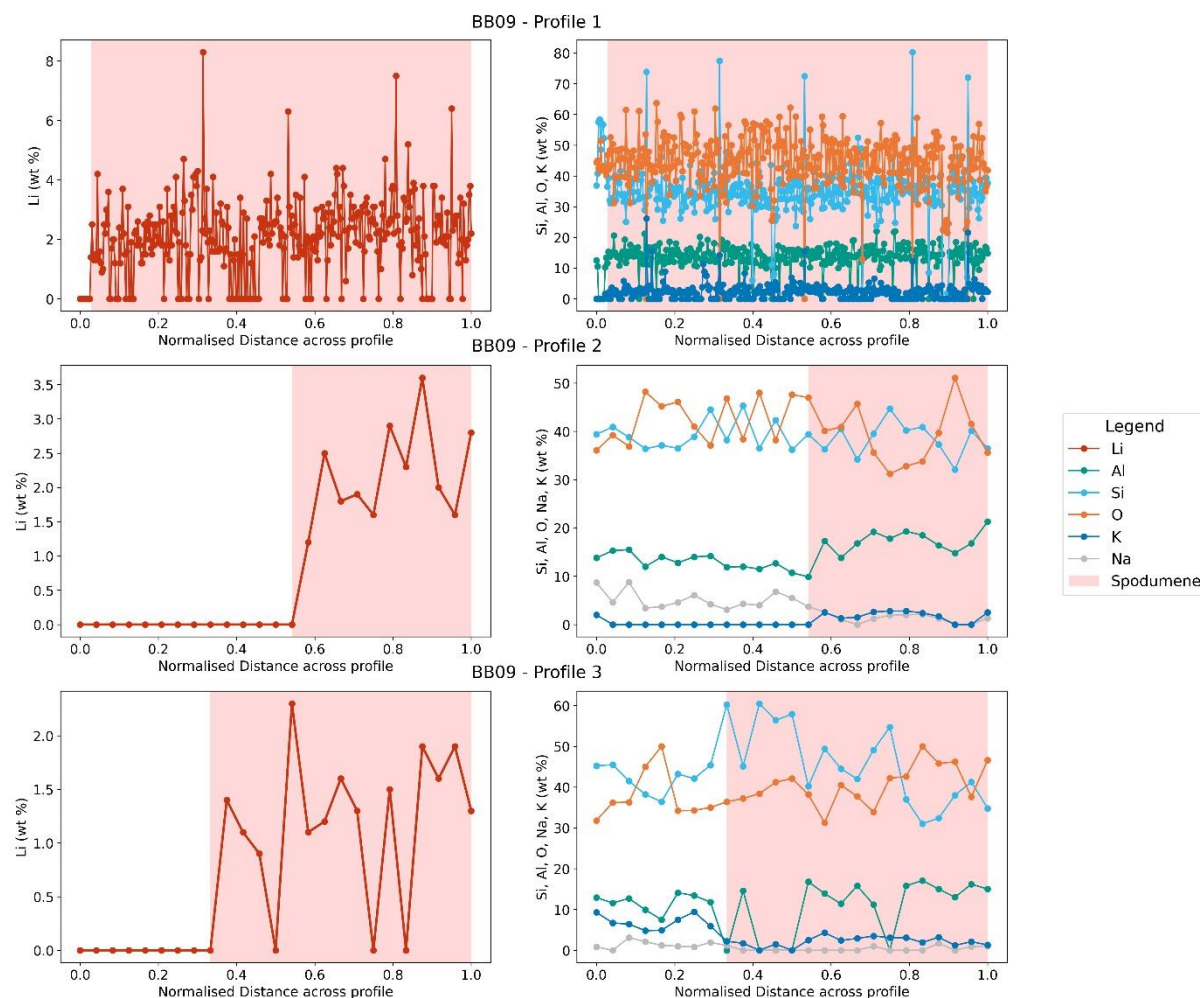


Figure E2. The entire profiles for sample BB09 from the block sample. Li, Al, Si, O, Na and K wt % is plotted against the normalised distances for each profile. The points recorded in the spodumene crystal are within the red shaded areas.

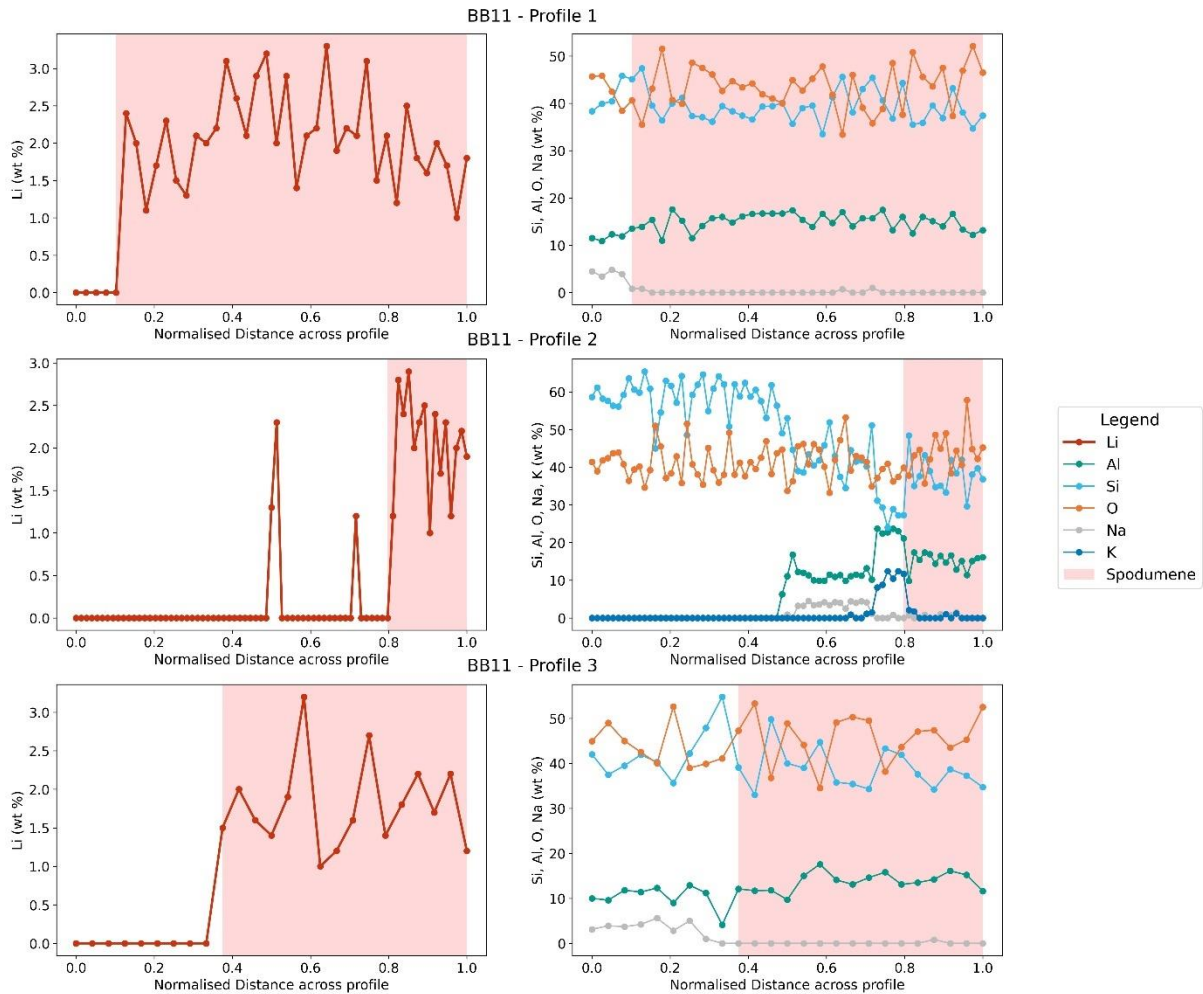


Figure E3. The entire profiles for sample BB11 from the block sample. Li, Al, Si, O, Na and K wt % is plotted against the normalised distances for each profile. The points recorded in the spodumene crystal are within the red shaded areas.

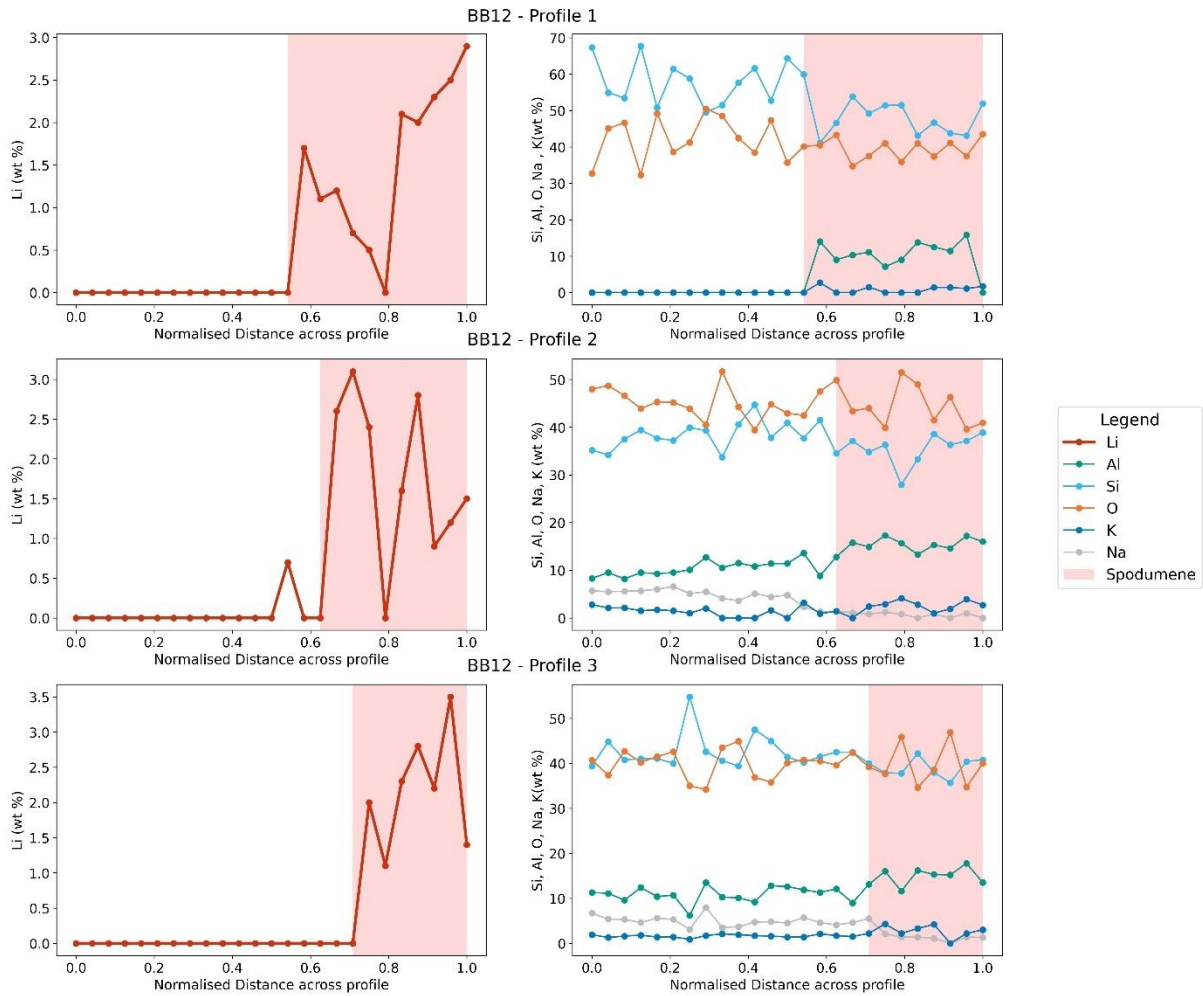


Figure E4. The entire profiles for sample BB12 from the block sample. Li, Al, Si, O, Na and K wt % is plotted against the normalised distances for each profile. The points recorded in the spodumene crystal are within the red shaded areas.

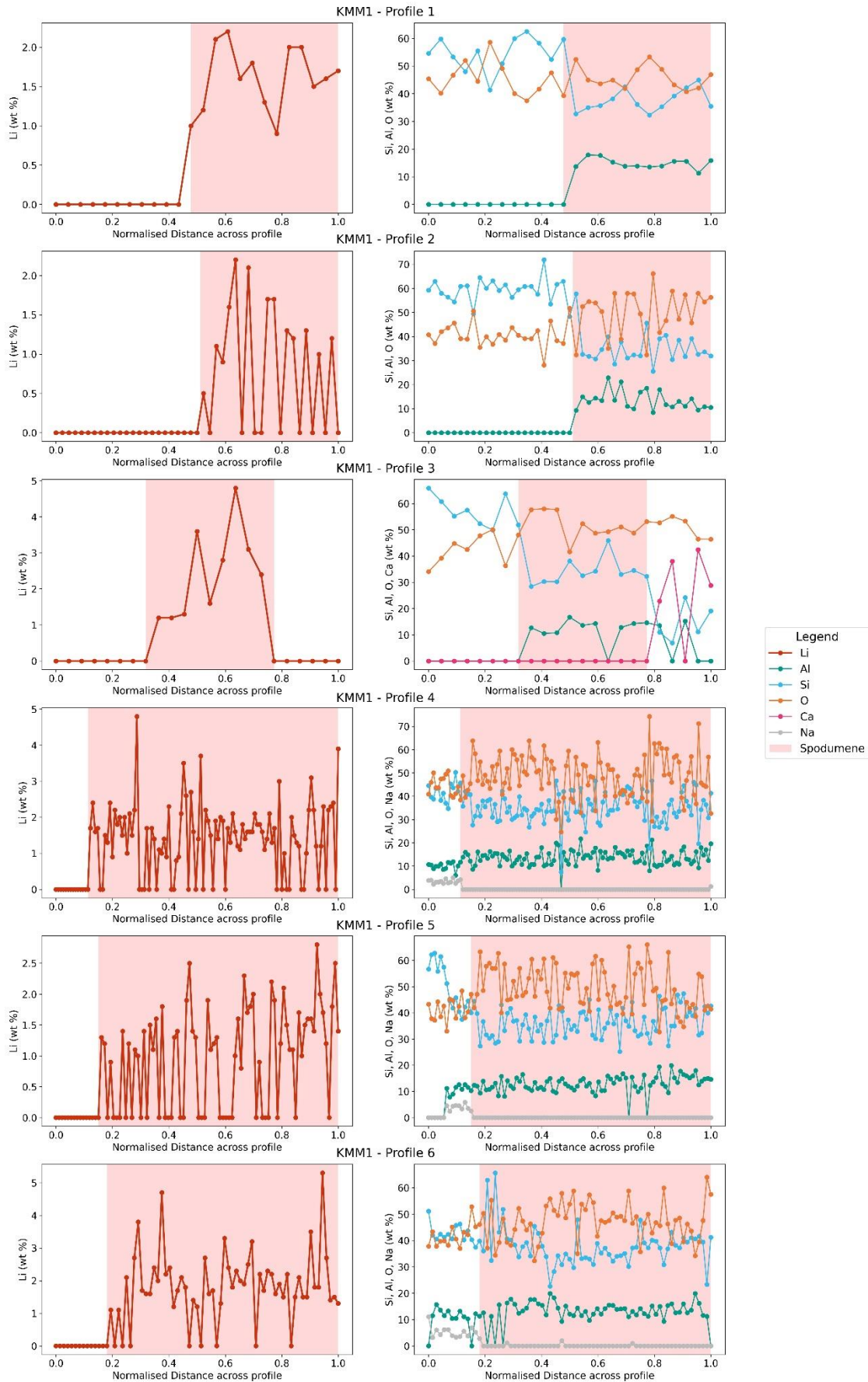


Figure E5. The entire profiles for sample KMM1 from the block sample. Li, Al, Si, O, Na and Ca wt % is plotted against the normalised distances for each profile. The points recorded in the spodumene crystal are within the red shaded areas.

Appendix F: All LIBS profiles for the Thin Sections

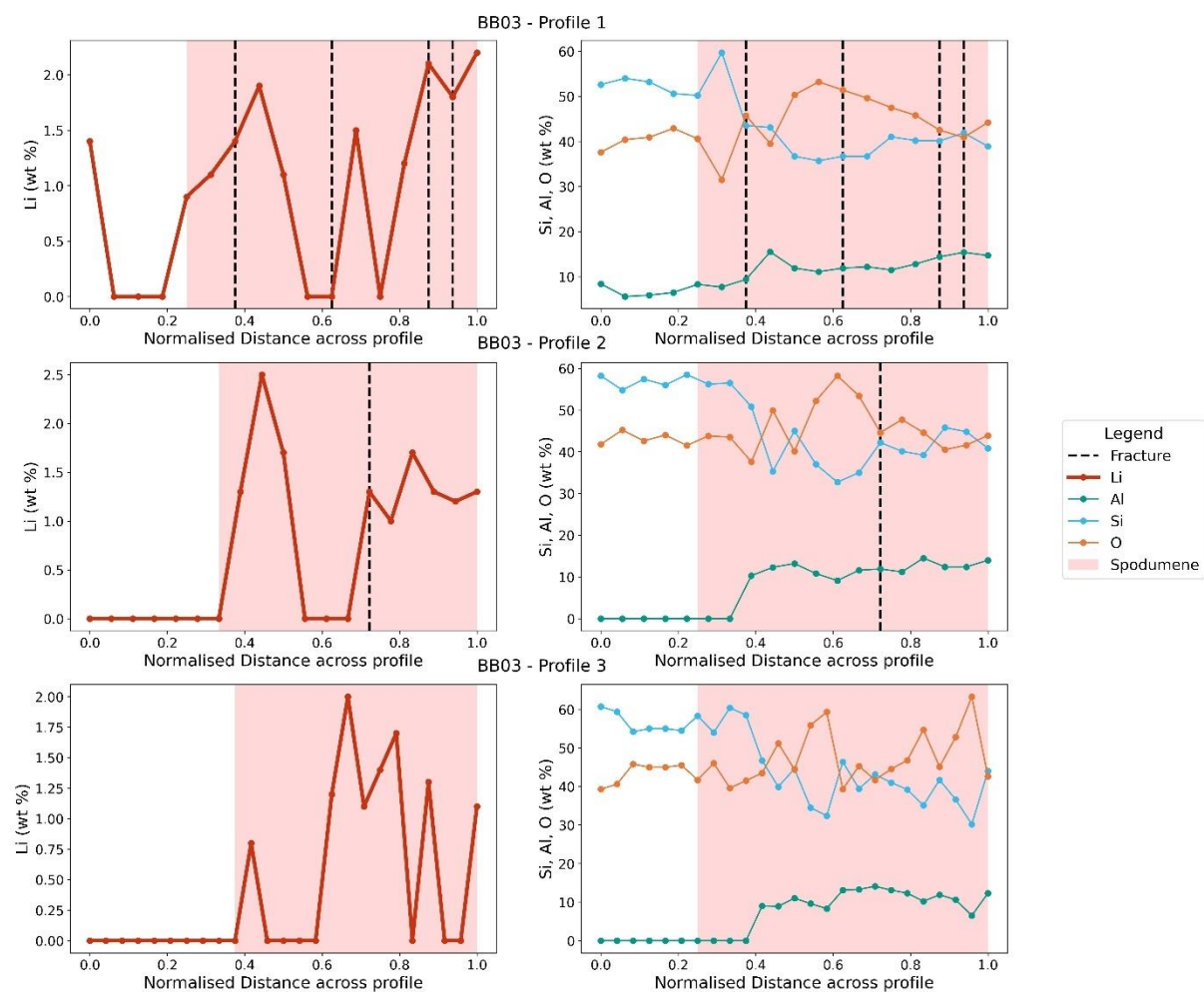


Figure F1. The entire profiles for sample BB03 from the thin sections. Li, Al, Si, and O wt % is plotted against the normalised distances for each profile. The points recorded in the spodumene crystal are within the red shaded areas. Any fractures or cleavage planes are indicated by black dashed lines.

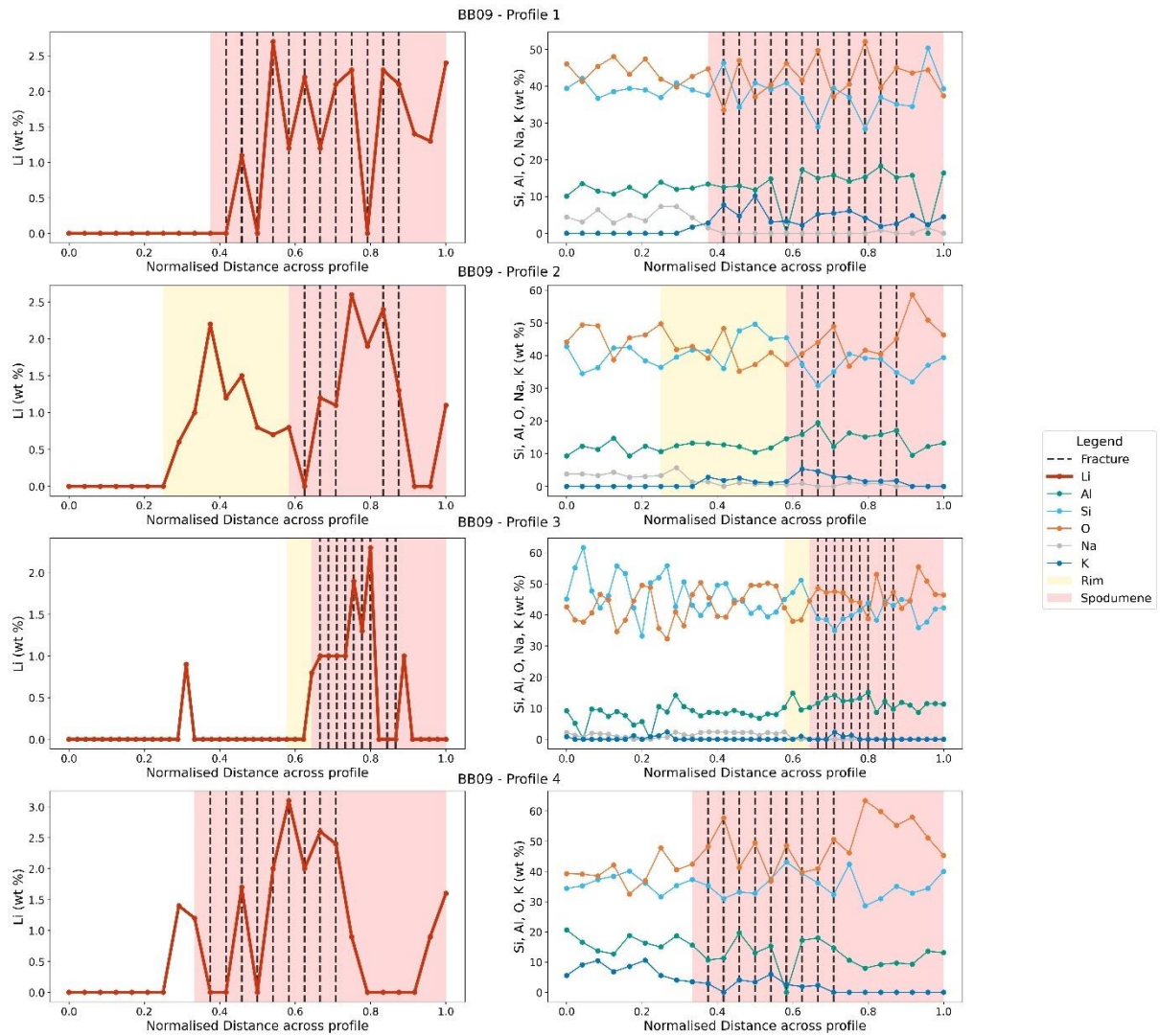


Figure F2. The entire profiles for sample BB09 from the thin sections. Li, Al, Si, O, Na and K wt % is plotted against the normalised distances for each profile. The points recorded in the spodumene crystal are within the red shaded areas. Rims around the spodumene crystal are indicated by the yellow shaded areas. Any fractures or cleavage planes are indicated by black dashed lines.

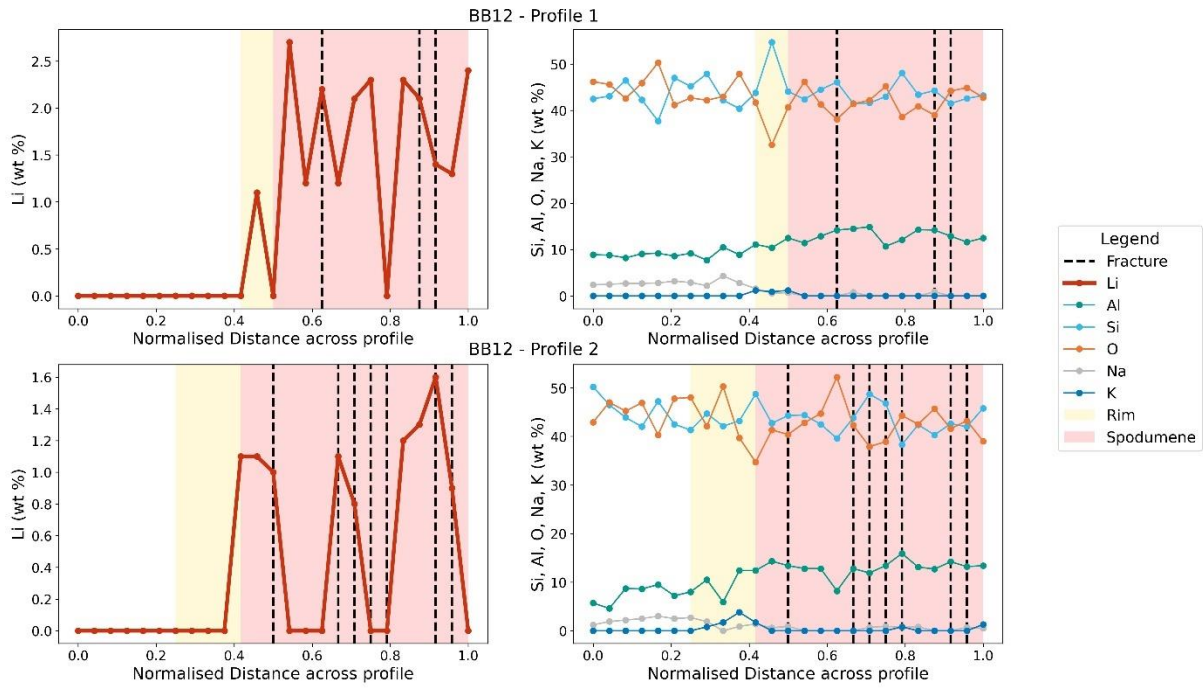


Figure F3. The entire profiles for sample BB12 from the thin sections. Li, Al, Si, O, Na and K wt % is plotted against the normalised distances for each profile. The points recorded in the spodumene crystal are within the red shaded areas. Rims around the spodumene crystal are indicated by the yellow shaded areas. Any fractures or cleavage planes are indicated by black dashed lines.

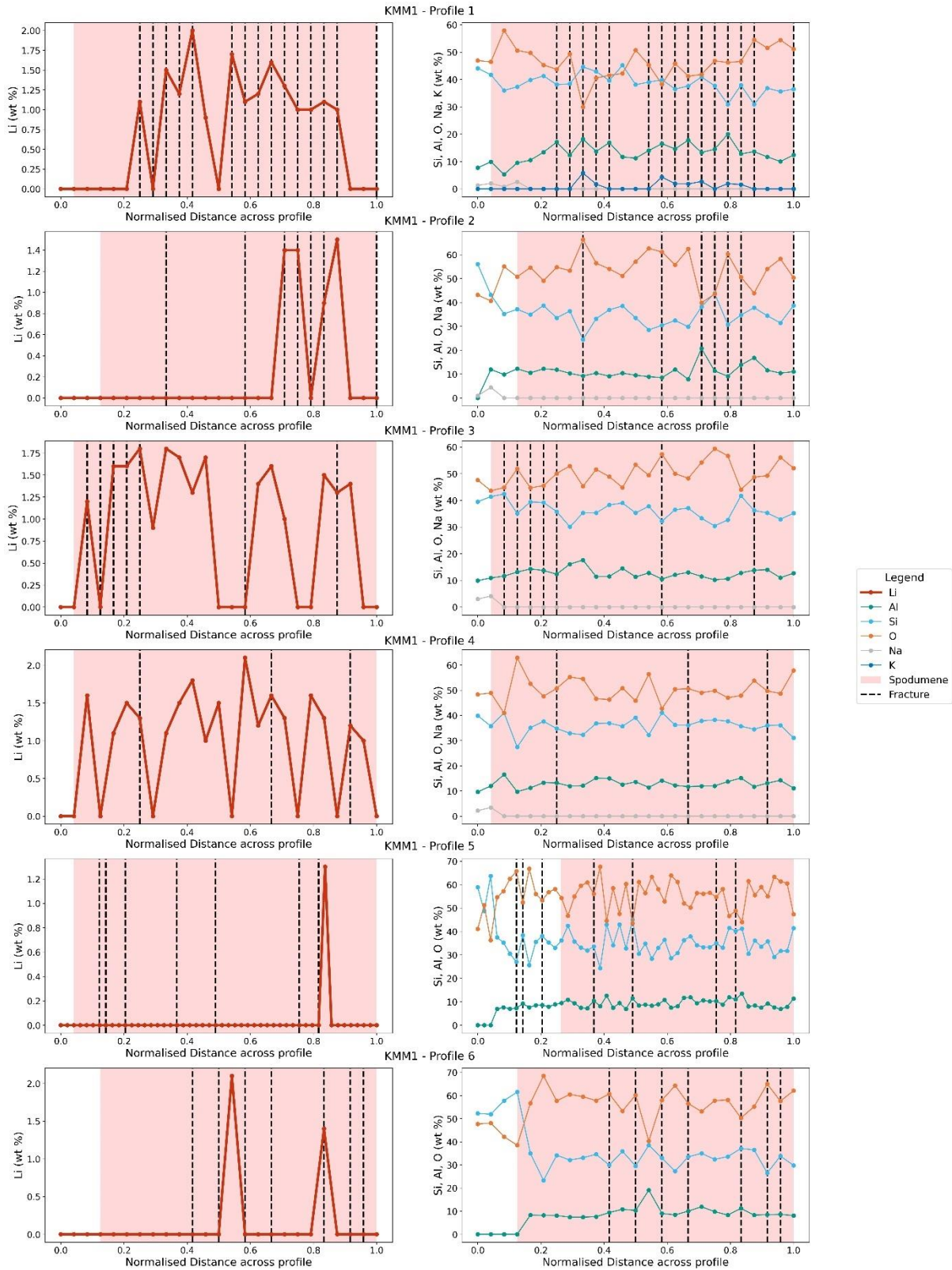


Figure F4. The entire profiles for sample KMM1 from the thin sections. Li, Al, Si, O, Na and K wt % is plotted against the normalised distances for each profile. The points recorded in the spodumene crystal are within the red shaded areas. Any fractures or cleavage planes are indicated by black dashed lines.

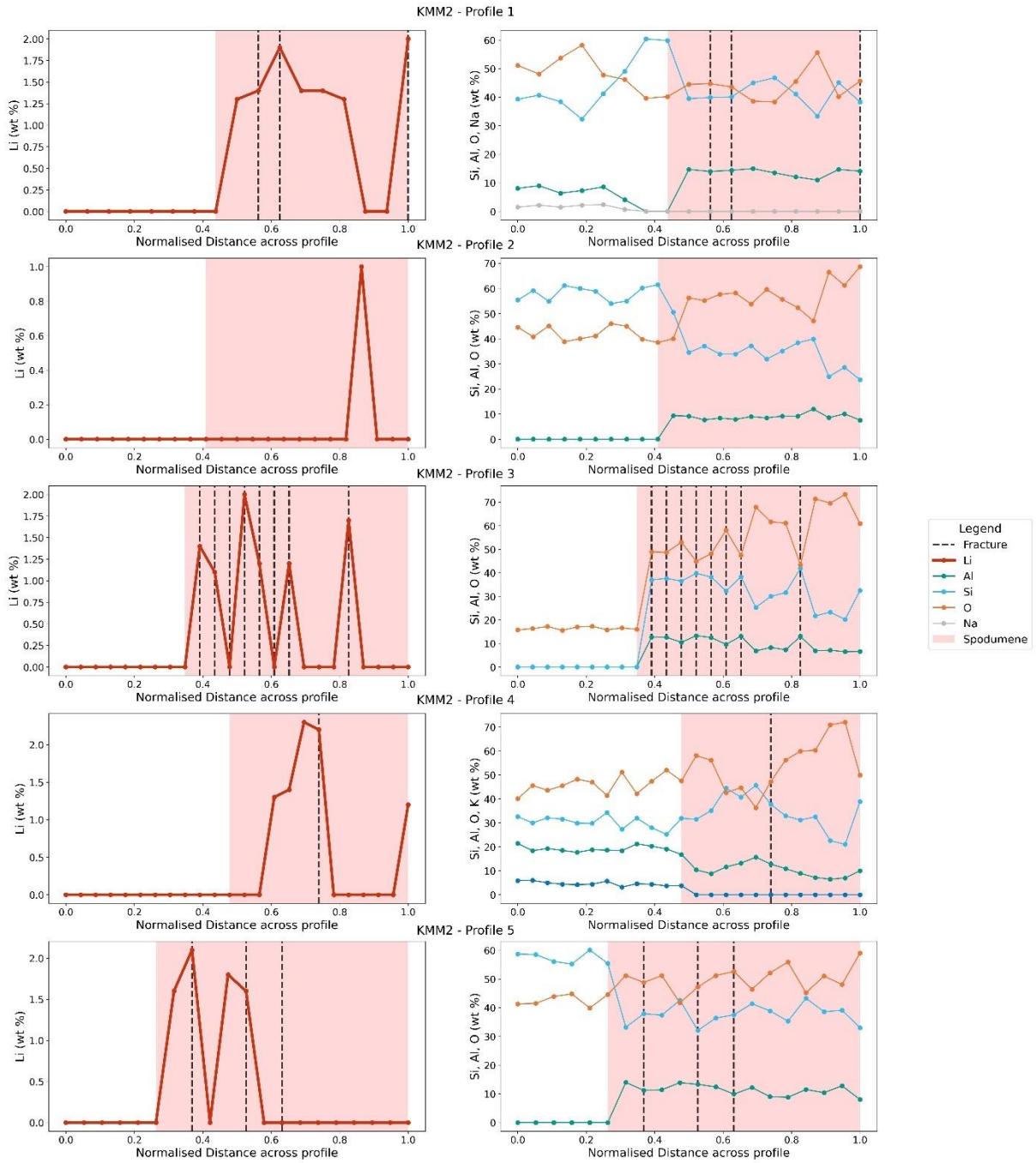


Figure F5. The entire profiles for sample KMM2 from the thin sections. Li, Al, Si, O and Na wt % is plotted against the normalised distances for each profile. The points recorded in the spodumene crystal are within the red shaded areas. Any fractures or cleavage planes are indicated by black dashed lines.